Advances in Water Resources 124 (2019) 120–138

Contents lists available at ScienceDirect

Advances in Water Resources

journal homepage: www.elsevier.com/locate/advwatres

On the linkage between runoff generation, land drainage, soil properties, and temporal patterns of precipitation in agricultural floodplains

Giulia Sofia [a,b,*], Francesca Ragazzi [c], Paolo Giandon [c], Giancarlo Dalla Fontana [b], Paolo Tarolli [b]

[a] Department of Civil & Environmental Engineering, University of Connecticut, 261 Glenbrook Rd, Storrs, CT 06269, United States
[b] Department Land, Environment, Agriculture and Forestry, University of Padova, Viale dell'università 16,Legnaro, (PD) 35020, Italy
[c] ARPAV Soil Protection and Remediation Service, via S. Barbara 5/A, Treviso I-31100, Italy

ARTICLE INFO

Keywords:
Soil
Infiltration
Lidar
Green-Ampt
Runoff
Flood

ABSTRACT

Accurate awareness of how rainfall, land use changes, and soil types control water fluxes in agricultural floodplains remains a crucial challenge in water resource research. This study examines soil moisture conditions, soil texture and rainfall characteristics, together with different artificial drainage network structures covering a time-span of 100 years (1924–2010), as drivers for runoff production in an agricultural floodplain. The research incorporates a multiple-layer generalised Green-Ampt approach to simulate water infiltration into the ground. Once the storage offered by the soil is saturated, a portion of the surface storage provided by the drainage network satisfies the infiltration capacity, thus delaying runoff. The watershed response is defined by the *uNSI* (updated Network Saturated index, (Sofia and Tarolli, 2017), that indicates the moment the available storage (soil + network) is 100% saturated. The results highlighted how interlocking relations between soil properties, the geometry of the network and temporal variations of precipitation determine runoff generation timing. For short return times, intense rainfalls tend to produce a quicker response in areas with soils prone to saturation, and with decreased network complexity. However, when the event magnitude increases, this combination of soil and network structure produces the fastest response when rainfall is more regular. Intense events in zones with soils with higher permeability produce a quicker response the simpler the network is. When soils are prone to runoff, and the network efficiency increases, runoff production is delayed in time. When soils have elevated permeability, and the network has a reduced efficiency and path heterogeneity, increasing the network simplicity would result in similar outcomes. Moreover, if the path heterogeneity and network efficiency increases, for a given network sinuosity, runoff generation would be delayed. Quantifying these effects is indeed crucial for many environmental problems, including the prediction of impacts of a changing climate and land use and the associated pressures.

1. Introduction

In a changing climate, weather events are expected to generate an increasing number of floods, threatening urbanised landscapes (Sofia et al., 2017; Zhang et al., 2012) and increasing people vulnerability (Roder et al., 2017). Many factors affect runoff processes, and they can influence flood management and prediction. The most important are topography, soil properties and land use (Kalantari et al., 2014). Amongst human modifications of topography, drainage networks are one of the vital components of the landscape. They have traditionally been linked with important human settlements throughout history (Chin et al., 2013; Ellis, 2011; Gregory, 2006; Hooke, 2006; Macklin and Lewin, 2015; Ruiz-Constán et al., 2017; Yevjevich, 1992; Zhang et al., 2015). Especially in floodplains, due the negligible topographic gradients and possible interactions between overland and channel flows (Viero et al., 2014), the network structure and its properties strongly modify runoff production and flood developments (Ibbitt, 1997; Saco and Kumar, 2002; Seo et al., 2015; Seo and Schmidt, 2012; Sofia et al., 2014; Sofia and Tarolli, 2017; Surkan, 1969; Zhang et al., 2015). Together with drainage networks and land use (Brath et al., 2006; Krause et al., 2007; Niehoff et al., 2002; Schilling and Helmers, 2008; Ungaro et al., 2014; Wheater and Evans, 2009), soil properties play a fundamental role in runoff production (Cerdà, 1998; Lado et al., 2004; Xiao et al., 2015). At the local scale, infiltrability and surface soil permeability (or field saturated hydraulic conductivity (Bouwer, 1966; Scherpinski et al., 2010)) activate surface and near-surface flow paths (Elsenbeer, 2001). Thus, these properties control dominant storm flows, and they provide a preliminary understanding of runoff generation when linked with rainfall characteristics (Bonell and Bruijnzeel, 2009). Further critical drivers of runoff are soil moisture conditions, soil texture and rainfall characteristics, especially

* Corresponding author at: Department of Civil & Environmental Engineering, University of Connecticut, 261 Glenbrook Rd, Storrs, CT 06269, United States.
E-mail address: giulia.sofia@uconn.edu (G. Sofia).

https://doi.org/10.1016/j.advwatres.2018.12.003
Received 25 June 2018; Received in revised form 2 November 2018; Accepted 12 December 2018
Available online 13 December 2018
0309-1708/

in semiarid catchments (Casenave and Valentin, 1992; Cerdà, 1998; Malik et al., 1987). The interaction between human activity and natural system dynamics, while inherent to civilisation, has dramatically conditioned the evolution of landscapes since ancient times (Tarolli et al., 2018; Tarolli and Sofia, 2016), influencing both soils, topography and flood aggressiveness (Sofia et al., 2017). Furthermore, when analysing the timing of river floods in Europe over the past 50 years, clear patterns can be found of changes that can also be ascribed to climate effects (Blöschl et al., 2017), dominated mostly by multidecadal variability rather than by long-term trends (Hodgkins et al., 2017). However, the effects of various storm characteristics on rainfall-runoff coupled with imperviousness at the scale of small urbanised systems have not been fully determined (Guan et al., 2016; Qin et al., 2013; Yao et al., 2016). Identifying the hydrological consequences of these drivers (network properties and climate) is complicated, and requires detailed and accurate data (Fang et al., 2012; van den Elsen et al., 2003). Quantifying these effects is crucial for many environmental problems, including the prediction of impacts of a changing climate and land use and the associated pressures, but also in the transport of solutes and contaminants (Botter et al., 2010; Rinaldo et al., 2011).

The purpose of the study described in this paper is to use a simple, physically based model to examine the hydrological consequences of various storm characteristics coupled with soil characteristics (texture, antecedent moisture condition) and drainage network structures (covering a time-span of 100 years) on runoff production. The paper purposely focusses on soil and network properties, without considering the influence of land use and land cover. The research aims to disentangle inter-storm variability, landscape (soil) and human drivers in runoff production. More specifically, rather than discussing the importance of each driver as single predictor, this research highlights their importance and interaction in the complex system of a floodplain agricultural area.

2. Materials and methods

2.1. Study area

The research area covers about 30 km^2, and it belongs to two municipalities in the Province of Padua (Veneto, North-Eastern Italy): Megliadino San Vitale and Megliadino San Fidenzio (Fig. 1). The study site is bounded by administrative boundaries, not by watershed divides. In this floodplain landscape, the definition of a topographic watershed is very complex, and since most of the flows are mechanically controlled, each pumping station defines an independent sub-unit where flows are constrained. The area is about 70 km south-west of Venice and 35 km south-west of Padua. It is mostly flat (avg slope is 2.9°), and it is a typical example of the diffuse city environment (Besussi et al., 1998; Fabian, 2012). It is part of the Holocenic plain formed by the Adige and Agno-Guà-Frassine rivers. The landscape is mostly agricultural, with some spotted urbanised areas that have increased in the last ten years mostly following the road network shape. The main agricultural activities include vineyards, olive orchards, and crop cultivations, with more intensive crop and vines production near the urbanised areas. The available topographic information is a LiDAR Digital Terrain Model (DTM) surveyed in 2008–2010 (horizontal accuracy of about ± 0.3 m and vertical accuracy of ± 0.15 m) (Fig. 1a), together with historical maps from 1924 to estimate past drainage network (courtesy of Consorzio di bonifica Adige-Euganeo) (Fig. 1b and 1d), and a classification of soils for the whole location (Fig. 1c).

The soils are characterized by a certain degree of heterogeneity, ranging from fine silty Inceptisols (Oxyaquic Haplustepts) to coarse texture Entisols (Typic Ustipsamments) to soil rich in organic carbon (Fluventic Hapludolls) or with buried organic horizons (Table 1) (ARPAV, 2015).

The available soil information stems from pedotransfer functions (PTFs) based on actual properties of the soil matrix, including bulk density, organic matter and soil texture (ARPAV, 2011). For soils with clay 0%–49% and sand 0%–50%, local authorities applied the (Ungaro et al., 2005) PTFs derived from benchmark soils in the Pianura Padano–Veneta, Northern Italy. Outside the mentioned texture ranges, the soil water retention is evaluated from PTFs defined by (Rawls et al., 2003), calibrated on field surveyed values of percentage of clay, sand and organic carbon; the hydraulic conductivity derives from PTFs calibrated on clay, sand and bulk density according to (Brakensiek et al., 1984).

2.2. Network characterisation

A correct characterisation of the drainage network is essential to predict the likely responses of flooding to the large-scale changes in the complexity of the drainage system induced by changes in socio-economic drivers. The study site was divided into subareas of 250 m × 250 m, to capture the geometry of the network and permanent variations in soil sealing (urban expansion). Three parameters characterise the irrigation network: storage capacity, drainage density, and fractal dimension. While storage capacity and drainage density are mostly related to irrigation needs, we assumed the fractal dimension to be representative of changes in the network shapes due to changes in agricultural mechanisation and field properties. Thanks to the availability of a high-resolution Lidar DTM, it has been possible to identify and characterise the current drainage network (Cazorzi et al., 2013) automatically. The approach is direct and straightforward, and it is based on a 'detrending technique'. The topographic information is filtered using a low pass filter, resulting in a smoothed surface to subtract from the original Lidar DTM (Cazorzi et al., 2013). As the height in the detrended data represents a height difference from a smoothed surface, positive peak values highlight microtopographic elements in the landscape, in this case, the drainage network. Hence, a statistic threshold can be applied to extract the features of interest. For each extracted element, it is possible to estimate a width and length, and thus aggregate this information to estimate an average channel width and subsequently the water storage per areal units. Please refer to (Cazorzi et al., 2013; Sofia et al., 2014) for a detailed description of the procedure.

For the past network, we digitalised the drainage channels from historical maps from 1924 (Gazzin, 2017). For each subarea, we assumed an average channel cross-section equal to the mean value estimated for the year 2010 (Sofia et al., 2014). Water storage volumes were then estimated starting from the network length and cross-section area for each section.

To better describe the river networks, in this paper, the fractal dimension (*FD*) for each network is estimated by applying box-counting approach (Backes and Bruno, 2012; Coelho and Costa, 1996). To evaluate the *FD*, square boxes with side length ε were generated and placed over the network. The number of boxes, $N(\varepsilon)$, in which a part of the fractal falls, is then counted. $N(\varepsilon)$ increases with the decrease of the size of the box. The fractal dimension *FD* is then the slope of the relationship between log (ε) and log $N(\varepsilon)$ according to Eqution.

$$\log N(\varepsilon) = -FD \log(\varepsilon) + C$$

where C is a constant of proportionality which allows for the relationship between N and ε (Zhang et al., 2015).

For this study case, we evaluated *FD* for each 250 m x 250 m subarea. Thus the size of the box varied from 1 to 250 m.

To reduce the high variability, the changes in the network characteristics (storage capacity $\Delta Stor_{cap}$, drainage density $\Delta Drain_d$, fractal dimension ΔFD) between the two reference years (2010–1924) have been classified into four classes (Fig. 2g,h,i) named Low (L), Medium Low (ML), Medium High (MH) and High (H). The classes were defined according to a Natural Breaks Classification, seeking to minimise each class's average deviation from its mean, while maximising each class's deviation from the means of the other groups. Each class indicates the

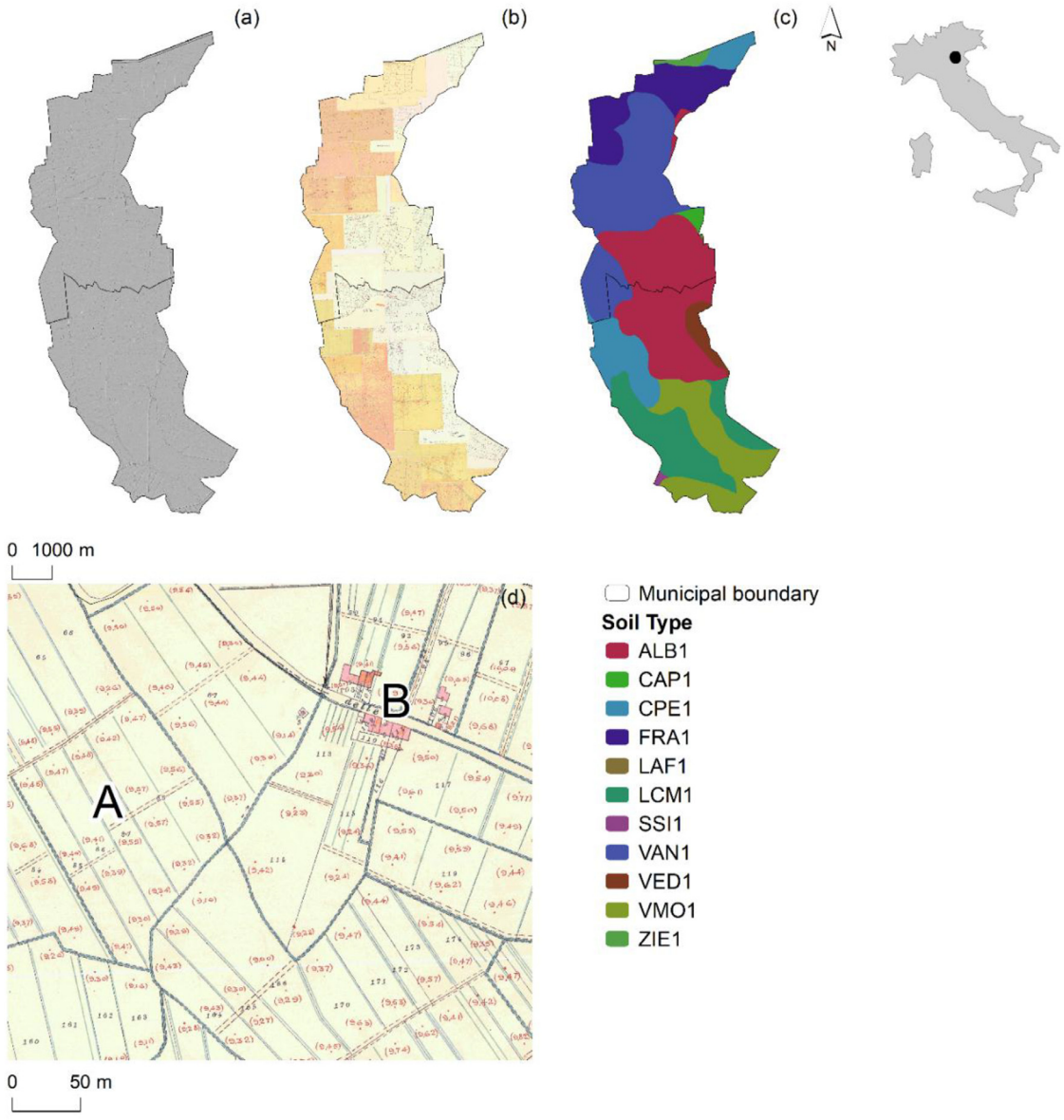

Fig 1. Study area with available Lidar DTM (a), mosaic of historical maps from 1924 (b) and soil types (c). An example of the historical map (d) is presented, with highlighted the minor drainage network (A) and the urban areas (B).

differences between each parameter in 2010 respect 1924. High means much lower value of the parameter in 2010 respect 1924.

It is important to highlight that the Low and part of the Medium-Low class represent areas where the network properties increased in 2010 respect to the past. For the $\Delta Stor_{cap}$ and $\Delta Drain_{d}$ the change is towards the end of the ML class, while for ΔFD it is at the beginning of the ML class.

2.3. Rainfall-Runoff mechanism

This paper considers the updated Network Saturation Index (*uNSI*) (Sofia and Tarolli, 2017) that indicates the time needed for a designed rainfall to saturate the available storage volume, depending on the soil characteristics and antecedent moisture condition (AMC). See (Sofia and Tarolli, 2017) for the details. The basic steps applied for the evaluation of this index are: (i) create Depth-Duration Frequency –DDF- curves (see (Svensson and Jones, 2010) for a full review) to simulate synthetic rainfalls; (ii) simulate a reference rainfall with different hyetographs shapes; (iii) evaluate the infiltration to simulate the effective rainfall and runoff to compute the *uNSI*.

2.3.1. Storm and interstorm variability

To evaluate the effect of storm variability on the watershed response, regarding ponding time and the difference in *uNSI*, and to make a comparative analysis, we followed Sofia and Tarolli (2017) and we considered the same hyetographs of the referenced work (17 hyetographs). Hyetographs include: a dimensionless rainfall (Wilson et al., 2006), hyetographs for rainfalls of 1, 2, 4, 8, 24, 48, 72, 168, 240 h (Florida Department of Transportation, 2015), the SCS/NRCS hydrographs (type I (for a design storm of 24 and 48 h), type Ia (for 24 h), type II (for a design storm of 24 and 48 h) and type III (for 24 h)) (Cronshey, 1986), and two more hyetographs proposed for a rainfall of 72 and 96 h (St. Johns river water management district, 2010). Storms could assume multiple forms, and these hyetographs are mostly considered as reference example. To provide the possibility of generalising the results, we considered a qualitative characterisation of the interstorm variability. Sofia and Tarolli (2017) mathematically characterised the rainfall bursts within

Table 1
soil types for the study area, and relative parameters (ARPAV, 2015). Textural classes type refers to: Sand (S), Loamy Sand (LS), Silt Loam (SIL), Silty Clay Loam (SICL), Loam (L), Sandy Loam (SL), Loam (L), Silty Clay (CL), Clay (C). Horizon names are also reported [A: Mineral horizons that have formed at the soil surface and exhibit obliteration of the original rock structure and show an accumulation of humified organic matter and properties resulting from cultivation. Ap: A horizons with properties from tillage or other disturbance. Ab horizons: Buried genetic A. B: Horizons that have formed below an A horizon, dominated by the obliteration of all or much of the original rock structure. Bw: B horizons that show alteration with the development of color or structure, or both, with little or no apparent illuvial accumulation of material. Bk: B horizons with accumulation of secondary carbonates. C: Horizons or layers, excluding strongly cemented and harder bedrock, that are little affected by pedogenic processes. Most are mineral layers. Cg: C horizons showing strong gleying.].

		ALB1				VAN1				CAP1	
Horizon name		Ap	Bw	Bk	Cg	Ap	B w	Bk	C	Ap	C
textural class		SIL	SIL	SIL	SIL	L	SL	SL	SL	SL	S
Soil depth (cm)	D	50.00	80.00	115.00	150.00	50.00	70.00	100.00	150.00	55.00	150.00
Saturated moisture content	θ_s	0.41	0.40	0.41	0.42	0.41	0.42	0.41	0.44	0.42	0.51
Wetting front suction head	Ψ_f	23.00	31.00	36.00	54.00	16.00	14.00	19.00	5.00	11.00	3.00
Hydraulic conductivity (cm/h)	K^t	0.024	0.038	0.049	0.072	0.107	0.186	0.060	1.396	0.370	4.053

		CPE1			LCM1			SSI1			
Horizon name		Ap	Bw	C	Ap	Bkg	Cg	Ap	Bw	Ab	Cg
textural class		CL	L	L	C	L	SIL	SICL	SIL	SICL	SIL
Soil depth (cm)	D	50.00	90.00	150.00	50.00	85.00	150.00	50.00	90.00	110.00	150.00
Saturated moisture content	θ_s	0.42	0.42	0.43	0.45	0.40	0.41	0.41	0.41	0.41	0.42
Wetting front suction head	Ψ_f	18.00	19.00	25.00	64.00	32.00	48.00	46.00	49.00	56.00	58.00
Hydraulic conductivity (cm/h)	K^t	1.800	1.900	2.500	0.009	0.059	0.098	0.074	0.043	0.051	0.073

		FRA1				ZIE1			
Horizon name		Ap	Bw	Ab	Cg	Ap	Bw	Ap	Cg
textural class		SICL	SICL	SICL	SICL	SICL	SICL	SICL	SIL
Soil depth (cm)	D	45.00	75.00	90.00	150.00	50.00	90.00	120.00	130.00
Saturated moisture content	θ_s	0.43	0.44	0.51	0.44	0.41	0.41	0.41	0.43
Wetting front suction head	Ψ_f	56.00	62.00	68.00	79.00	71.00	46.00	61.00	59.00
Hydraulic conductivity (cm/h)	K^t	0.033	0.033	0.037	0.002	0.054	0.045	0.061	0.063

		VED1			VMO1		
Horizon name		Ap	Bw	Cg	Ap	Bw	2Ckg
textural class		L	L	L	SICL	SICL	SICL
Soil depth (cm)	D	50.00	90.00	150.00	50.00	85.00	135.00
Saturated moisture content	θ_s	0.41	0.41	0.43	0.42	0.41	0.44
Wetting front suction head	Ψ_f	18.00	24.00	46.00	49.00	87.00	68.00
Hydraulic conductivity (cm/h)	K^t	0.034	0.041	0.060	0.107	0.044	0.015

the storm, where a burst is an abrupt change in rainfall rate (Huff, 1967). The authors defined four criteria, specifically: (i) the time, in percentage of the total, to the heaviest burst ($BrLoc_{\%}$); (ii) the number of bursts (Br_n); (iii) the shape of the hyetograph (*TRN*), as in the ratio between the hyetograph area and the area of a triangle having as base the hyetograph duration, and as height, the height of the main rainfall burst. (iv) the asymmetry of the storm volumes (*asym*), defined as the ratio between the amount of rainfall fell before the maximum burst and that after the burst.

We qualitatively classified each rainfall parameter (Table 2) according to a Natural Breaks Classification. For this classifications, asymmetry has been defined as Negatively Skewed (NS), Right-Centred (RC), Left-Centred (LC), and Positively-skewed (PS), *TRN* has been defined as Low (L), Medium-Low (ML), Medium-High (MH) and High (H), $BrLoc_{\%}$ has been defined as Beginning (B), first half (FH), second half (SH) and end (E). Furthermore, Br_nhas been defined as single peak (SP) or multi-peaks (MP). Fig. 3 shows a descriptive example of the different qualitative measures.

These criteria highlight some climatic characteristics. Changes in $BrLoc_{\%}$ can simulate changes in climate to heavy rainfalls beginning earlier (Abbs, 1999) within a storm. The contribute of intense rainfall events (Cortesi et al., 2012; Sofia et al., 2017; Zhang et al., 2009) can be simulated according to different $Br_n$and *TRN*. As well, *TRN* and asymmetry can simulate the effect of rainfall non-uniformity, a critical element increasing flooding (Wasko, 2014; Wasko and Sharma, 2015).

For simulation purposes, it is necessary to define a rainfall duration. (Sofia and Tarolli, 2017) considered the time needed for a rainfall to fill the available superficial storage capacity. Their work did not account for infiltrated water to define this timing. In this study, since we have different soil types, we decided to focus on a duration able to produce an *effective* rainfall (rainfall minus infiltration) able to fill the 90th percentile of the storage volumes available in 1924. Storage capacity (volume) is a distributed value (one value per subarea of 250 m × 250 m) thus some local peaks might be related to outliers or locally extracted areas: by considering the 90th percentile of these values, we ensure the effective rainfall to have a realistic duration and amount. To obtain the rainfall duration, we simulated an 'average dry soil type', defining a soil having as hydraulic parameters an area-weighted average of the parameters of each available soil in the study area, and an initial moisture content of 0. To define the rainfall duration, we re-created a variable rate pattern based on average characteristics of storms defined by the whole set of hyetographs, and we selected the time producing an average rainfall intensity (average considering all the possible hyetographs) able to saturate the first layer of the abovementioned 'average dry soil type'. For this study, the storm time (t) is 6.4 h, and the rainfall cumulated amount refers to that derived for $t = 6.4$ h and DDF curves for a return time of 2,5,10,30,50,100,200 years.

2.3.2. Generalized Green-Ampt model

Previously (Sofia and Tarolli, 2017), the infiltration had been investigated considering a single layer of soil, and a single soil type. However,

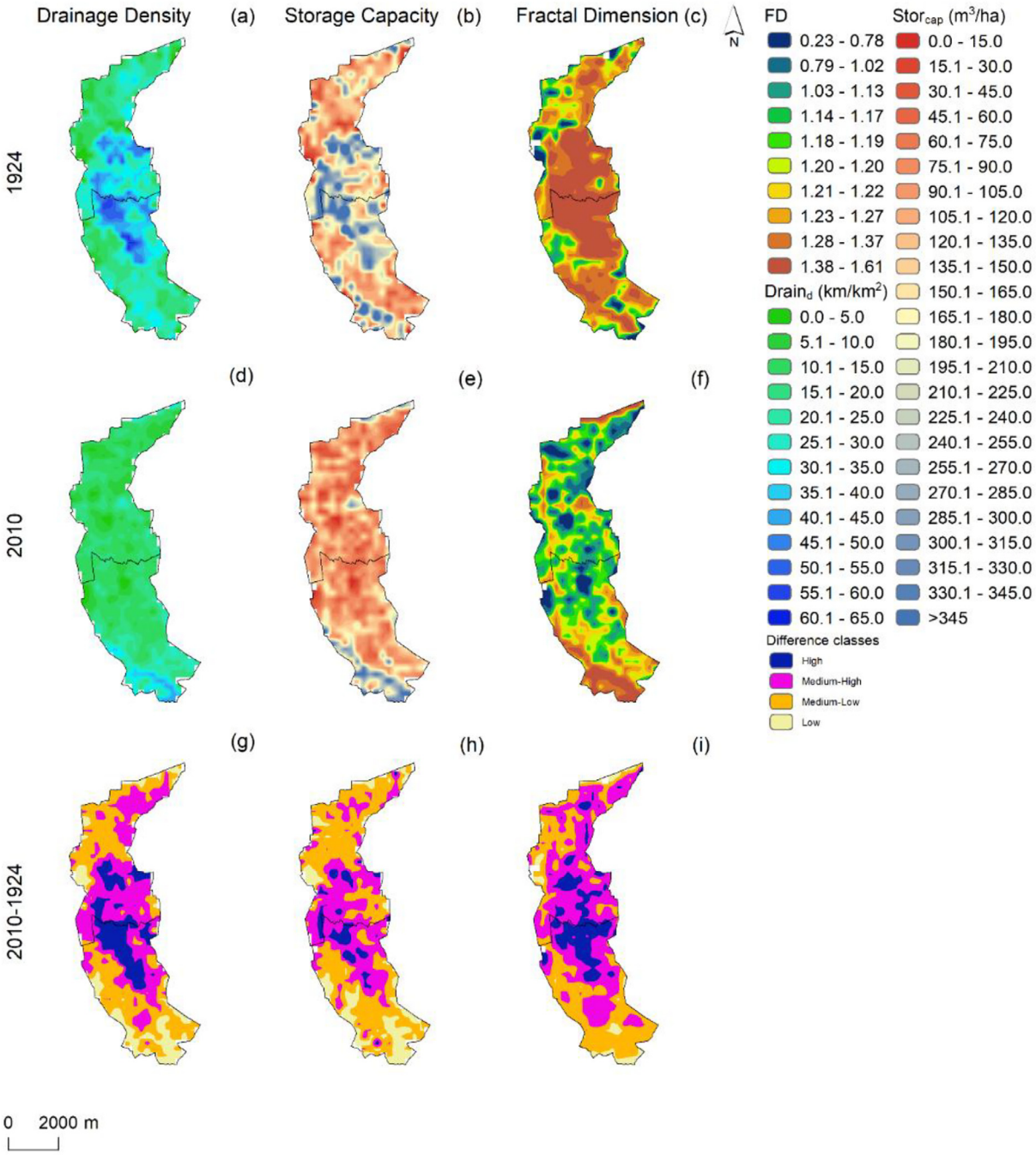

Fig. 2. Characterization of the networks in 1924 and 2010 (storage capacity $Stor_{cap}$, drainage density $Drain_d$, fractal dimension FD) and relative differences between the years.

in nature, layered soils are the norm rather than the exception. Independently from the number of layers, when a wetting front moves from one layer to the next, the infiltration rate will be reduced due to (i) reduced hydraulic conductivity (if a wetting front moves from a more porous to a less porous layer), (ii) reduced wetting front suction (in the opposite scenario). Furthermore, if the soils in the lower layers are much coarser than the top ones, the wetting front may become unstable and reduce the infiltration substantially (Downer and Ogden, 2003). For this reason, this work applies a generalised version of Green and Ampt (1911) approach. Here, the effect of layering is addressed averaging the soil properties based on the depths of the layers (Downer and Ogden, 2003).

The same basic assumption of the Green-Ampt model applies, that is that of a sharp wetting front. As the wetting front crosses the layers, the model assumes an instantaneous change in the initial moisture content, porosity and wetting front suction head. For a cumulative infiltration at the t time step ($F(t)$) in a layered soil with a total depth of D_{tot}, composed of i layers, each one having a specific hydraulic conductivity (K_i cm/h), depth (D_i cm), moisture deficit ($\Delta\theta_i$, as in the difference between the saturated water content θ_s and the initial water content θ_i), the effective hydraulic conductivity at the time-step t is evaluated as

$$K^t = \frac{\left(D_1 + \frac{F(t) - D_1 \Delta\theta_1}{\Delta\theta_2}\right)}{\left(\frac{D_1}{K_1} + \frac{\frac{F(t) - D_1 \Delta\theta_1}{\Delta\theta_2}}{K_2}\right)} \quad \text{when } z \leq D_1 \tag{1}$$

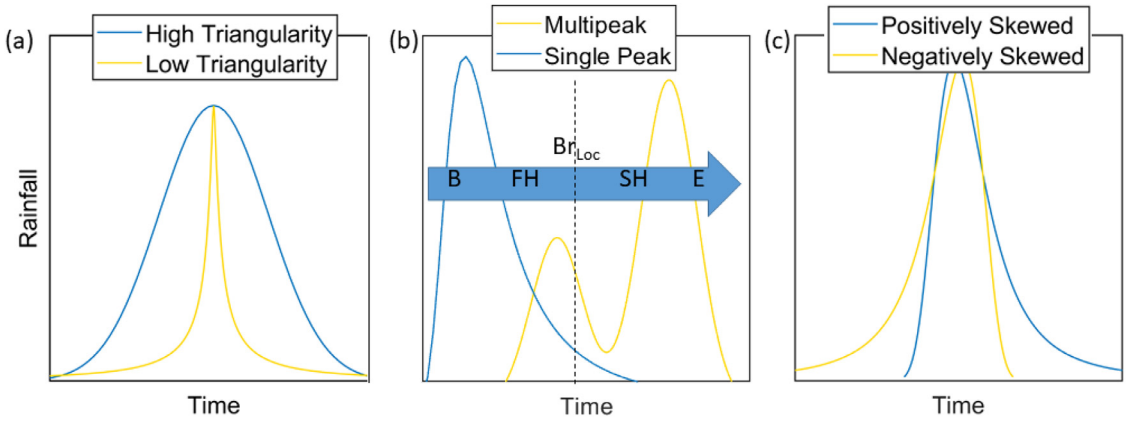

Fig. 3. Qualitative schematisation of the different hyetograps: (a) High or Low Triangularity (Medium High, and Medium Low would be intermediate measures between the two displayed); (b) Single or Multipeak, and location of the peak (B-Beginning, FH/SH- First or Second Half, E- End); (c) Positively or Negatively skewed. Dotted line represent half of the rainfall duration in time. The location of the peak, as displayed in (b) is defined for any hyetograph type, and it is measured for the heaviest burst of the rainfall (in the case of multipeak rainfalls). Similarly, the asymmetry is only displayed in (c), but it is evaluated for any event, single or multipeak ones, and to rainfall having different triangularity.

Table 2
Classification of the hyetographs according to the four defined criteria: location of the heaviest burst within the storm period ($BrLoc_{\%}$), percentage of the total storm period that has occurred at the start of the heaviest burst ($BrLoc_{\%}$), number of bursts (Br_n), hyetograph triangularity (*TRN*), asymmetry of the storm (*asym*). Asymmetry has been defined as Negatively Skewed (NS), Left-Centred (LC), Right-Centred (RC), and Positively-skewed (PS); $BrLoc_{\%}$ has been defined as Beginning (B), First-Half (FH), Second-Half (SH) and End (E), *TRN* has been defined as Low (L), Medium-Low (ML), Medium-High (MH) and High (H), and Br_nhas been defined as single peak (SP) or multipeak (MP).

	$BrLoc_{\%}$	Br_n	*TRN*	*asym*
Sym01	FH	SP	MH	RC
Sym02	FH	SP	H	RC
Sym03	B	SP	H	RC
Sym04	FH	SP	H	NS
Sym05	B	SP	MH	NS
Sym06	FH	SP	H	NS
Sym07	SH	MP	MH	LC
Sym08	E	MP	MH	PS
Sym09	SH	MP	ML	RC
Sym10	B	SP	ML	NS
Sym11	B	SP	ML	NS
Sym12	B	SP	MH	NS
Sym13	FH	SP	L	NS
Sym14	FH	SP	L	RC
Sym15	FH	SP	L	RC
Sym16	SH	SP	L	RC
Sym17	SH	SP	L	RC

$$K^t = \frac{\left(\sum_{n=1}^{i-1} D_n + \frac{F(t) - \sum_{n=1}^{i-1} D_n \Delta\theta_n}{\Delta\theta_i}\right)}{\left(\sum_{n=1}^{i-1} \frac{D_n}{K_n} + \frac{\frac{F(t) - \sum_{n=1}^{i-1} D_n \Delta\theta_n}{\Delta\theta_i}}{K_i}\right)} \quad \text{when } D_{tot} \geq z > D_1 \tag{2}$$

with z being the depth of the leading wetting front evaluated as $D_{i-1} + \frac{F(t)}{\Delta\theta_i}$ (Flerchinger et al., 1988)

That is, while the front is in the first layer, the hydraulic conductivity at any time, K^t, is equal to K_1, the hydraulic conductivity of the first soil horizon. When the leading edge passes the first layer, the effective hydraulic conductivity is calculated based on the depth of the leading edge of the wetting front (z), as a harmonic mean of the wetted layers (Downer and Ogden, 2003).

The cumulative infiltration, solved iteratively using the Newton Raphson method (Upton et al., 2008), at the $t+1$ time level is Chow et al. (1988) is

$$F^{t+1} = F^t + K^t \Delta t + {}_f\Delta\theta \ln\left(\frac{F^{t+1} + {}_f\Delta\theta}{F^t + {}_f\Delta\theta}\right) \tag{3}$$

The infiltration rate is

$$f^{t+1} = K^t\left(\frac{{}_f\Delta\theta}{F^{t+1}} + 1\right) \tag{4}$$

where ψ_f is the wetting front suction head and $\Delta\theta$ is the moisture deficit of the layer containing the leading front.

If at any timestep the rainfall intensity is higher than infiltration capacity (f^t), the excess rainfall will first fill the surface storage and then contribute to surface runoff. Thus, a significant parameter is the ponding time (Eq. (5)), or the time at which infiltration stops and runoff starts. For a storm of a specific duration and intensity (P), t_p is given by

$$t_p = \frac{K_i \psi_f (\theta_s - \theta_i)}{P(P - K_i)} \tag{5}$$

Where K and $\Delta\theta$ are the effective conductivity and the moisture deficit of the layer containing the leading front, and ψ_f is the wetting front suction head.

The local authorities (ARPAV, 2015) provided the input required for the Green-Ampt model (Table 1). Changes in the surrounding environment dynamically alter the hydraulic conductivity of the soil matrix. Therefore, the infiltration parameters for the Green-Ampt equation should change for each storm event (Risse et al., 1995). Different saturation (0%, 25%, 50%, 75%, 90%, 100%) were simulated to account for changes in the soil due to the antecedent soil moisture conditions (AMC), as

$$\theta_i = \theta_s \times m, \text{with } m = 0.00, 0.25, 0.50, 0.75, 0.90, 1.00 \tag{6}$$

with θ_s = saturated moisture content; and θ_i = initial (antecedent) moisture content.

2.4. Statistical inference

2.4.1. Return time and saturation vs ponding time and uNSI

According to (Sofia and Tarolli, 2017), ponding time and $\Delta uNSI$ vary depending on the event return period or the saturation condition following

$$y = ae^{(bx)} \tag{7}$$

with y being the Ponding Time (t_p) or the $\Delta uNSI$, x being the return period or the saturation condition, and a and b two empirical coefficients of different magnitude.

For this study, we tested the same hypothesis fitting the proposed equation to the $\Delta uNSI$ and ponding times evaluated in each subarea within the study site having a homogeneous soil type (the areas represented in Fig. 1c). The fitting was accomplished by a non-linear approximation approach based on a Gaussian model. In this method, the parameters of the approximating functions are not necessarily linear on the original function, and they are determined using non-linear optimisation (Dennis et al., 1996). The fitting automatically calculates optimised start points for Gaussian models based on the fitted dataset and imposes no bounds on the resulting coefficients. Further, we tested the value of R^2 for each fitted equation with a two-tailed Student's t-test for statistical significance at $\alpha = 0.05$. This procedure is implemented to verify if the (Sofia and Tarolli, 2017) also applies when infiltration is evaluated using a multi-layer Green-Ampt approach, and to verify the effects of different soil types. The fitted values of a and b have been classified according to a Natural Breaks Classification. Assessing changes in the coefficients it is not an easy task: identifying significant variations between coefficients, given their order of magnitude, is challenging. Classifying them into classes of high/low values ensure a greater understanding of the data, and highlights differences better. As a consequence, the results will be discussed addressing a and b as Low (a_L, b_L), Medium-Low (a_{ML},b_{ML}), Medium-High (a_{MH},b_{MH}) and High (a_H,b_H). a and b fitted for t_p have been plotted together to define hydrological similarities between the different soils. We applied a k-means clustering algorithm (David and Vassilvitski, 2007) to partition the soils into three main groups. The k-means clustering, for its simplicity and speed, is a widely used iterative, data-partitioning algorithm that minimises the average squared distance between points in the same cluster (David and Vassilvitski, 2007).

2.4.2. Quantifying differences

The influence of the hyetographs shapes, soil types and network parameters on ponding time or $\Delta uNSI$ was tested using multiple linear regression models, considering each criterion as a single predictor or implying an interaction among them. Statistically, an interaction describes a situation in which the simultaneous influence of two variables on a third is not additive. Given the high number of variables (four storm parameters and three network parameters), this research aimed to optimise the best subset of predictors to explain the watershed response: redundant predictors should be removed to explain the data most simply and effectively, and to reduce collinearity. Moreover, unnecessary predictors would merely add noise to the estimation of the ponding time and $\Delta uNSI$, rather than explaining them. Thus, as a novel step respect to Sofia and Tarolli (2017), we consider the Akaike information criterion (AIC) (Akaike, 1987, 1981; Pan, 2001) as an estimator of the relative quality of the statistical model for each given set of data. Given a collection of models for the data, the AIC forward-backwards selection estimates the quality of each model, relative to each of the other models. All the assumptions for the regression models were checked and, in the case of non-linearity between explanatory and response variables, a boxplot transformation was applied. Further, the Cook distance (Cook, 1979) was used to remove outliers when needed. We tested the presence of serial correlation among the residuals, and when present, the Durbin-Watson (DW) test (Durbin and Watson, 1950) at $\alpha = 0.05$ confirmed or declined the significance of the relationship given by the analysis of variance (ANOVA) results. The significance threshold level for the ANOVA was set to $p < 0.05$.

3. Results

3.1. Ponding time vs return period and saturation

Eq. (7) was fitted to the values of ponding time (tp) as a function of the return period –Rp- (Fig. 4a) or saturation –Sat.- (Fig. 4b). Table 3 reports the estimated a and b coefficients obtained for each soil type, as well as the goodness of fits.

When considering the relationship with the return period (Fig. 4a, Table 3) testing the value of R^2 for this equation with a two-tailed Student's t-test at $\alpha = 0.05$ shows there is a significant relationship between the two variables. As observed for a different soil in Sofia and Tarolli (2017), the return period has a weaker influence on ponding. At the increase of the magnitude of the event (increasing Rp), the saturation time always decreases. Observing the coefficients of $t_p = f(Rp)$, for the same return period, soils with a_L would saturate quicker than soils having a_H. However, differences arise depending on the magnitude of the events. The response of soils in a_L are not that marked for the lowest return periods (Rp 2 year), while they are highly evident (a saturation 60% faster) for the less frequent events (Rp 200 year). For a similar b, soils having a_L display a higher sensitivity to changes in the return period. The less frequent event (Rp 200 year) would result in a decrease of the ponding time of about 1 h and a half (−63%) for soils with a_L, whereas for soils having a_H, the same change would result in an anticipation of the ponding time of about 1 h (−40%). The values of b assume the highest value for the mostly sandy soil CAP1, and the lowest value for the soil LCM1 (with clay in the upper horizon). Changes in b result in similar changes in ponding time, independently from the return period, with soils in b_L having a quicker saturation (−60%) respect soils in b_H. However, changes in the return period from a frequent (Rp 2 year) to a rare (Rp 200 year) event, for a similar a, would result in higher changes in ponding time for soils having b_H respect to soils having b_L (1.5 h vs 50 m respectively).

Observing a and b together (Fig. 4a) the k-means algorithm define three groups (G1, G2 and G3), according to variations in ponding time Vs. Return period. a_L and b_L bound the first group (G1) that includes LCM1, VED1 and ALB1. ALB1 is the soil with Silty-Loam texture in all horizons (Table 1). LCM1 has clay in the first horizon, loam in the second and silty-Loam in the third, while VED1 presents Loam in all horizons (Table 1). The second group (G2) is bounded by a_{Md} (Medium-Low/Medium-High) and b_{Md} (Medium-Low/Medium-High), and it comprises CPE1, FRA1, VAN1. CPE1 presents Clay Loam or loamy horizons, FRA1 Silty-clay Loam, and VAN1 has loamy horizons closer to the surface, or sandy-loam horizons in depth. The third group (G3) has a_H and b_{MH-H}, and it includes SS1, ZIE1, VMO1 and CAP1. SS1 presents Silty clay loam horizons alternated to Silt loam horizons; ZIE1 presents Silty clay loam texture up to about 120 cm of depth, and then Silt Loam. VMO1 is entirely Silty clay loam, while CAP1 is sandy loam closer to the surface and sandy in depth.

According to the proposed model (Eq. (7)), and averaging a and b for each group, for the same return period, soils pertaining to G1 would saturate earlier in time, respect soils in G3, with slight differences depending on the frequency of the events (−22% for Rp 2 year vs −40% for Rp 200 year). The change in response due to the change in the event frequency (Rp 2 year to Rp 200 year) would be 60% more evident for soils in G1 vs soils in G3. This classification highlights how changes in the magnitude of the events have a more significant effect on ponding time than soil texture when taken as an independent parameter.

When considering saturation (Fig. 4b), testing the value of R^2 for this equation with a two-tailed Student's t-test at $\alpha = 0.05$ shows that, except for the soil CAP1, there is a significant relationship between the two variables. One must notice that CAP1 is the only soil characterised by a sandy texture. The lack of correlation between ponding time and saturation is mostly because a large number of the simulated hyetographs is not capable of saturating this specific soil for the considered rainfall duration. Observing the coefficients of $t_p = f(Sat)$, as expected, they show a negative correlation between ponding time and saturation, with a reduction of the ponding time at the increase of the soil moisture content. Lower values of a are related to soils having Silty-Loam textures, whereas a increases for soils having more uniform Silty-Clay-Loam textures, to reach the highest values for sandy soils. This defines more permeable soils (a_H) result in delayed ponding times Vs. more impervious

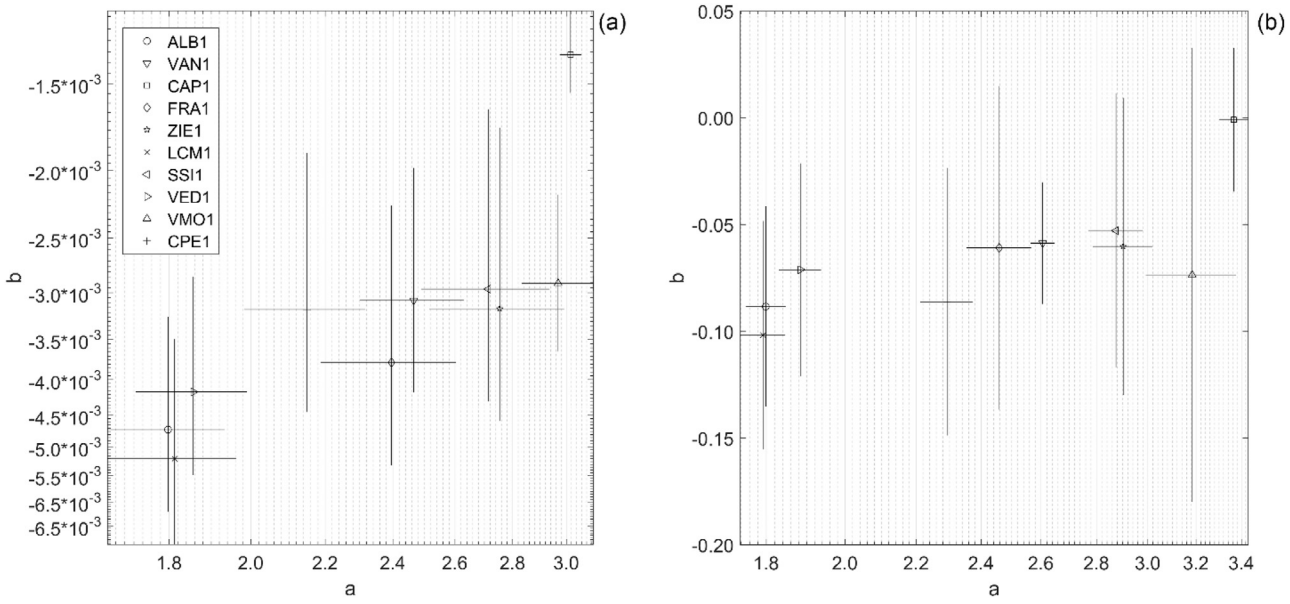

Fig 4. Coefficient of the power law equation for each soil type between ponding time and (a) return time and (b) saturation. 95% confidence bounds are also shown.

Table 3
Coefficients of Eq. (7) fitted considering ponding time (Pt) and saturation (Sat) or return period (Rp). 95% confidence bounds, R^2 and RMSE are also shown. Each coefficient has been classified according to a Natural Breaks Classification. The groups are labelled High (H), Medium-High (MH), Medium-Low (ML) and Low (L).

	$soil_G$	a	a $CI_{95\%}$	a levels	b	b $CI_{95\%}$	b levels	R^2	RMSE		
	Pt = f(Rp)										
'ALB1'	G1	1.80	1.66	1.93	L	−0.0047	−0.006	−0.003	ML	0.95	0.09
'VAN1'	G2	2.47	2.30	2.63	MH	−0.0031	−0.004	−0.002	H	0.93	0.12
'CAP1'	G3	3.02	2.98	3.06	H	−0.0014	−0.002	−0.001	H	0.99	0.03
'FRA1'	G2	2.40	2.19	2.60	ML	−0.0038	−0.005	−0.002	H	0.92	0.15
'ZIE1'	G3	2.75	2.52	2.99	H	−0.0032	−0.005	−0.002	H	0.89	0.17
'LCM1'	G1	1.81	1.66	1.96	L	−0.0052	−0.007	−0.004	L	0.95	0.10
'SSI1'	G3	2.71	2.49	2.94	MH	−0.0030	−0.004	−0.002	H	0.89	0.16
'VED1'	G1	1.86	1.72	1.99	L	−0.0042	−0.006	−0.003	MH	0.95	0.09
'VMO1'	G3	2.97	2.83	3.11	H	−0.0029	−0.004	−0.002	MH	0.96	0.10
'CPE1'	G2	2.15	1.98	2.32	ML	−0.0032	−0.005	−0.002	ML	0.91	0.12
	Pt = f(Sat)										
'ALB1'	G1	1.799	1.75	1.85	L	−0.088	−0.135	−0.042	ML	0.92	0.02
'VAN1'	G2	2.606	2.56	2.65	MH	−0.059	−0.087	−0.030	H	0.94	0.02
'CAP1'	G3	3.366	3.30	3.43	H	−0.001	−0.035	0.033	H	0.00	0.03
'FRA1'	G2	2.459	2.35	2.57	ML	−0.061	−0.137	0.015	H	0.69	0.04
'ZIE1'	G3	2.903	2.79	3.02	H	−0.060	−0.130	0.009	H	0.72	0.05
'LCM1'	G1	1.792	1.74	1.85	L	−0.102	−0.155	−0.048	L	0.92	0.02
'SSI1'	G3	2.875	2.77	2.98	MH	−0.053	−0.117	0.011	H	0.70	0.04
'VED1'	G1	1.884	1.83	1.94	L	−0.071	−0.121	−0.021	MH	0.87	0.02
'VMO1'	G3	3.184	2.99	3.38	H	−0.074	−0.180	0.033	MH	0.62	0.08
'CPE1'	G2	2.293	2.21	2.37	ML	−0.086	−0.149	−0.024	ML	0.86	0.03

soils, with an increase of about 70% in time, independently from the saturation.

Considering the parameter b, the lowest values (b_L) are related to LCM1, while the coefficient progressively increases to reach the highest values at the increase of the permeability or water retention capacity (FRA1,VAN1,LCM1,ZIE1,CAP1). Differences in b determine differences in response to the AMC. For the same saturation (Sat 0%), b_H Vs b_L results in an almost unnoticeable delayed response (–0.5%), whereas an almost saturated soil (Sat. 90%) would have a delay of ~5% in ponding time. As well, soils with b_H would result in a lower response to saturation changes, with about a ~4% delay in time changing from dry to saturated soils (Sat. 0% to 90%), whereas soils with b_L would result doubled time increase (~8%), for the same saturation change.

Considering both a and b (Fig. 4b), soils can be clustered together into three groups. The first group (G1) is bounded by a_L and $b_{L-ML,}$ and it includes LCM1, VED1 and ALB1. The second group (G2) is bounded by a_{ML} and b_{Md} (Medium-Low/Medium-High), and it comprises CPE1, FRA1, VAN1. The third group (G3) has a_{MH-H} and $b_{Md\text{-}H,}$ and it includes SS1, ZIE1, VMO1 and CAP1. Interestingly, this classification creates the same groups like the one for the return period equation coefficients, thus indicating how soil textures and hydraulic properties in general plays a similar role in soil response respect changes in AMC and magnitude of the rainfall event. According to the proposed model (Eq. (7)), and averaging a and b in each group, for the same saturation conditions, soils pertaining to G1 would saturate about 70% earlier in time, respect soils in G3, with slight differences depending on the soil moisture condition (69% for Sat. 0% vs 75% for Sat. 90%). Averaging, soils in G1 saturates in about 1 h and 45 min, Vs. soils in G3 that saturates in about 3 h. The change in response due to the change in saturation (Sat. 0% to 90%) would be 50% more evident for soils in G1 vs soils in G3. This classification highlights how changes in textures have a more significant effect on ponding time than AMC.

Table 4
P-values of the statistical significance of the percentage of the total storm period that has occurred at the start of the heaviest burst ($BrLoc_{\%}$), number of bursts (Br_n), hyetograph triangularity (*TRN*), asymmetry of the storm (*asym*) and their interaction (labelled with:) on the average ponding time (avg), or on the ponding time of each considered saturation (sat) and return period (RT). For clarity, only values with statistical significance at $p < 0.05$ have been reported.

	Sat. 0%				Sat. 50%			Sat. 90%		
	avg	2	50	200	2	50	200	2	50	200
$soil_G$	6E-17	3E-23	1E-29	6E-39	3E-49	1E-20	3E-44	3E-28	2E-25	3E-44
$BrLoc_{\%}$	6E-34	1E-29	2E-27	2E-10	1E-41	4E-12	8E-61	2E-21	6E-10	8E-61
TRN	9E-03	–	–	4E-18	5E-05	5E-07	2E-06	2E-05	5E-10	2E-06
asym	2E-04	–	1E-02	–	–	–	3E-04	–	–	3E-04
Br_n	–	2E-02	1E-02	–	4E-08	1E-02	1E-07	1E-02	–	1E-07
$BrLoc_{\%}$:TRN	3E-20	1E-13	3E-16	7E-03	2E-18	2E-09	2E-32	4E-14	1E-08	2E-32
Br_n:TRN	2E-10	4E-03	5E-06	2E-02	8E-06	4E-03	1E-09	4E-05	6E-03	1E-09
$BrLoc_{\%}$:asym	–	4E-02	–	–	2E-02	–	4E-02	–	–	4E-02
TRN:asym	–	4E-02	1E-02	–	3E-04	5E-02	2E-05	2E-02	–	2E-05
$BrLoc_{\%}$:TRN:asym	3E-11	1E-15	3E-16	–	1E-31	6E-03	3E-26	2E-09	–	3E-26
$soil_G$: $BrLoc_{\%}$	2E-06	1E-14	4E-20	5E-11	3E-40	3E-04	6E-35	3E-16	1E-02	6E-35
$soil_G$: Br_n	6E-04	6E-04	6E-04	6E-04	6E-04	6E-04	6E-04	6E-04	6E-04	6E-04
$soil_G$:TRN	7E-03	7E-03	7E-03	7E-03	7E-03	7E-03	7E-03	7E-03	7E-03	7E-03
$soil_G$: $BrLoc_{\%}$:TRN	1E-08	1E-08	1E-08	1E-08	1E-08	1E-08	1E-08	1E-08	1E-08	1E-08
$soil_G$: Br_n:TRN	0E + 00	0E + 00	0E + 00	0E + 00	0E + 00	0E + 00	0E + 00	0E + 00	0E + 00	0E + 00

3.2. Ponding time and interstorm variability

According to the AIC approach, the best fit model to represent the variations in ponding time is given by Eq. (8)

$$Ptime \sim Soil_G + BrLoc_{\%} + Br_n + TRN + asym + Soil_G : BrLoc_{\%} + Soil_G : TRN + Soil_G : BrLoc_{\%} : TRN + BrLoc_{\%} : asym + TRN : asym + BrLoc_{\%} : TRN : asym + Br_n : TRN + Soil_G : Br_n : TRN \quad (8)$$

The final model present a Residual standard error of 0.30 on 148° of freedom (DF), multiple R^2 of 0.91, Adjusted R^2 of 0.89, F-statistic: 67.36 on 21 and 148 DF and p-value: < 2.2E-16. Compared to the model before the AIC approach, Eq. (8) reduces the residual standard error (−0.01), increases the R^2 (+0.01), increases F (+20), and it increases the degrees of freedom (+10), thus effectively removing drivers excessive to estimate the parameters' variability.

The location of the heaviest storm burst ($BrLoc_{\%}$), the regularity of the rainfall intensity (*TRN*), the asymmetry of the rainfall volume (*asym*) have (in average) a statistically significant influence the ponding time (Table 4). While $BrLoc_{\%}$is always significant, independently from the magnitude of the events, and from the AMC, *TRN* becomes significant only for increasing saturation (Sat. >= 50%, Table 4), or for increasing magnitude on dry soils (Rp 200 year, Sat. 0%). *asym* is only significant for dry soils and average return periods (Sat. 50%, Rp 2 year, Table 4), or for rare events with increasing AMC (Sat >= 50%, Rp 200 year, Table 4). The number of bursts (Br_n) is only significant for dry soils and rather frequent events (Rp <= 50 year, Sat. 0%), always significant with average AMC, independently from the magnitude of the events, and it is significant for very rare (Rp 200 year) or rather frequent (Rp 2 year) events in saturated AMC (Sat. 90%).

Overall, early peak events ($BrLoc_{\%}$=B Vs E, Fig. 5) tend to reduce the ponding time. Negatively skewed hyetographs also determine a quicker runoff production overall. Rainfall intensity (*TRN* = L Vs H) also influence negatively the ponding time, and so do multipeak rainfalls, but only when intensity is high (*TRN* = Low). Interactions, in fact, arise. Independently from soil groups, the location of the peak, the asymmetry of the rainfall and its triangularity matter at all saturation and independently from the magnitude of the event (Table 4, Fig. 5a). Soil groups, on the other hand, interact with storm triangularity and peak location (Fig. 5b), and with triangularity and number of bursts (Fig. 5c), but the strength of this interaction changes with changes in saturation (Fig. 6). Runoff production is the quickest for intense storms (*TRN* = L) with early peaks ($BrLoc_{\%}$= B Vs E, Fig. 5a) and negatively skewed hyetographs (most of the rainfall volume falling before the bursts). A strong quickening in runoff production is also related to intense events (*TRN* = Low, Fig. 5b) and impervious soils (G1), especially for early peak storms ($BrLoc_{\%}$=E). Faster runoff productions are also related to impervious soils (G1) and intense (*TRN* = Low) multipeak (Br_n= MP) storms (Fig. 5c).

The type of correlation with ponding time, as described above, however, changes at different saturations (Sat) and return period (Rp) for the various predictors (Fig. 6).

The importance of soil groups as independent predictor decreases at the increase of saturation: moving from soils in G1 (more permeable) to G3 (less permeable) decreases the ponding time (Fig. 5), but these textural changes matter the most in low AMC (Sat <= 50%, Fig. 6). The predictor with the highest negative effect on ponding time is the number of peaks (Br_n), with the highest negative effect on ponding time in dry soils. The highest positive effect is given by the interaction between soil groups and number of peaks, especially in frequent events (Rp 2 year) and dry soils (Sat 0%), followed by the interaction between triangularity (*TRN*) number of peaks (Br_n). Increasing the magnitude of the events reduces the correlation between each predictor(s) and ponding time. Interestingly, there is a drastic shift in correlation between low magnitude events (Rp 2 year) and extreme ones (Rp 200 year) for the Soil ($Soil_G$ as single predictor, or interacting with others), the number of peaks (Br_nas single predictor, or interacting with others) and triangularity (*TRN* as single predictor, or interacting with others). For low magnitude events, the increase in saturation reduces the anticipation of ponding time at the changes in soil texture, at the increase of peak numbers and the more regular the events are. Differently, extreme events produce a quicker runoff at the increase of the peak number and of the intensity of the event.

3.2.1. Similarities with previous findings

Analysing the actual soil response without considering the network changes offers a starting point to understand future changes (Sofia and Tarolli, 2017). For this case study, focusing on soil response, the results underlined how changes in the magnitude of the events has a larger effect on ponding time than soil texture when taken as an independent parameter, while different texture classes have a larger effect on ponding time than AMC. The effect of texture on ponding time is also observed for other parts of the world, where initial soil moisture effects on the flood response have been shown to depend on event magnitude rather than on the climate or region properties (Grillakis et al., 2016). When considering interstorm variability, this research confirmed what found in Sofia and Tarolli (2017). The proposed analysis suggests that an expected quickening of the runoff production is related to rainfall having

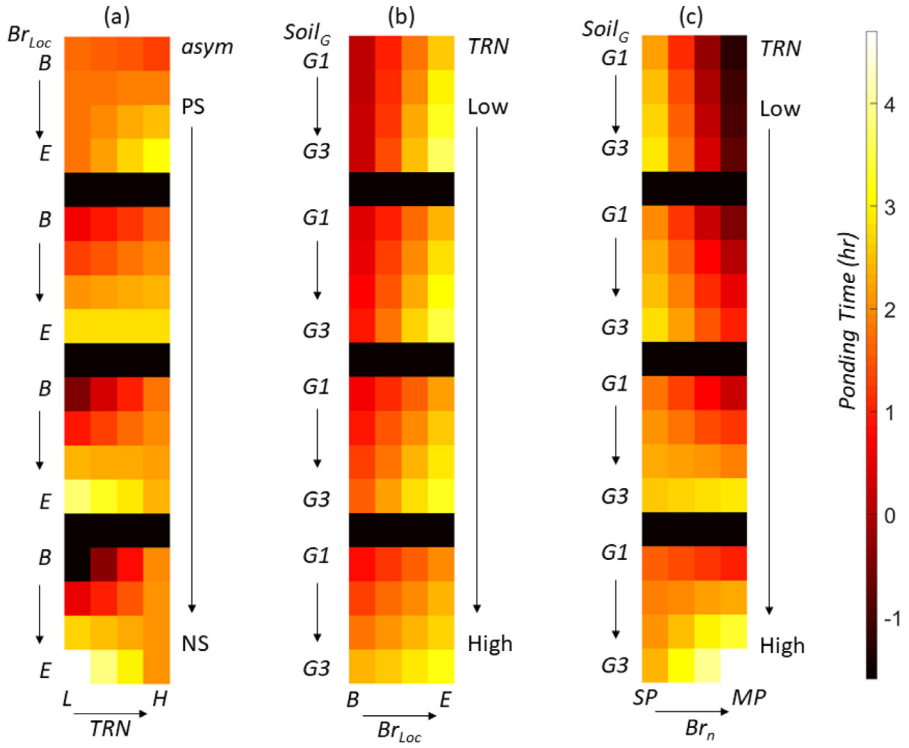

Fig. 5. The plots show the average (for all saturations and return periods) estimated effect on the response of the ponding time (in hours) from changing each predictor value: (a) $BrLoc_{\%}$: *TRN: asym* (b) $Soil_G$: $BrLoc_{\%}$: *TRN* and (c) $Soil_G$: Br_n: *TRN*. The considered predictors are asymmetry (*asym*), percentage of the total storm period that has occurred at the start of the heaviest burst ($BrLoc_{\%}$), triangularity (*TRN*) and Soil groups ($Soil_G$) defined as G1 and G3 according to chapter 3.1 (G2 is represented by intermediate pixels between these two). Asymmetry has been defined as Negatively-Skewed (NS), Right-Centred (RC), Left-Centred (LC), and Positively-skewed (PS). $BrLoc_{\%}$ has been defined as Beginning (B) and End (E), but intermediate pixels between the two represent FH and SH. *TRN* has been defined as Low (L), and High (H), but intermediate large squares between the two are Medium-Low (ML) and Medium-High (MH).

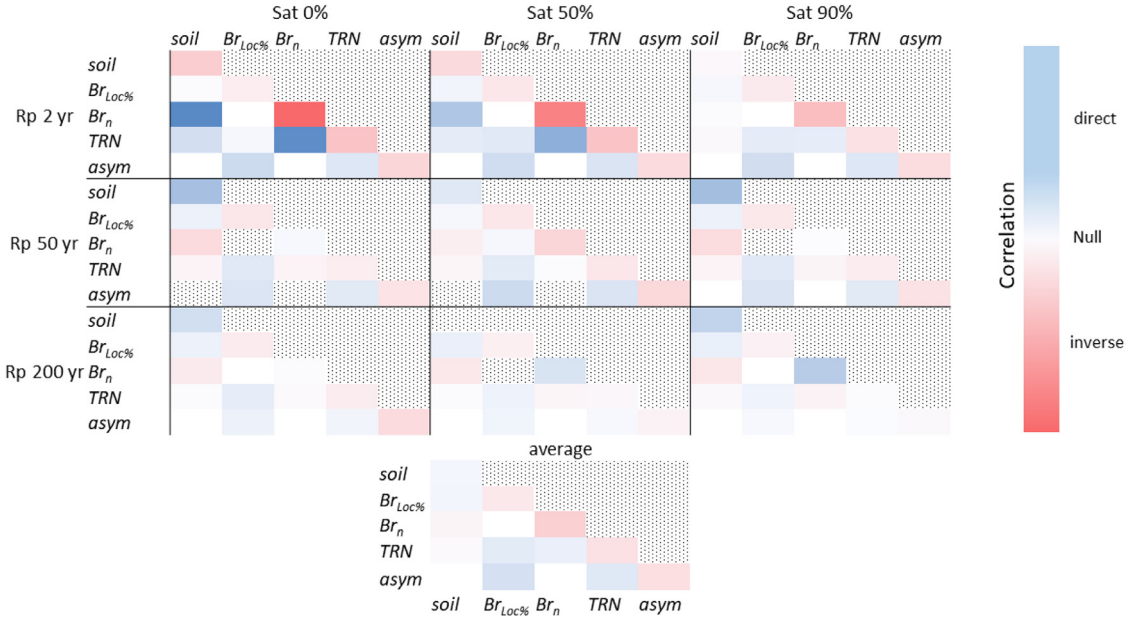

Fig 6. The plots show the correlation between ponding time (in hours) at different saturations (Sat) or return period (Rp) and the Number of bursts (Br_n), asymmetry (*asym*), percentage of the total storm period that has occurred at the start of the heaviest burst ($BrLoc_{\%}$), triangularity (*TRN*) and soil type and their two ways interaction. Red gradient toward darker colors imply a stronger inverse correlation, that is a change in the mentioned parameter(s) determine a decrease of the ponding time. Similarly, blue gradients towards lighter colors imply a stronger direct correlation, that is a change in the parameter(s) determine an increase of the ponding time. No correlation is represented in white (For interpretation of the references to color in this figure legend, the reader is referred to the web version of this article.).

a large intensity peak at the beginning of the storm, coupled with an increase of the volume of water falling before the heaviest burst and intensity of the event. The effects of the peak locations are in line with what found in the literature. (Zhang et al., 1997) reported that runoff was twice as large and quicker in 'early peak' events than in 'delayed peak' events that delivered the same total depth of rain in the same event duration. Similarly, when dealing with chemical losses on relatively dry soils (AMC ~6%), (Potter et al., 2006) found greater chemical loss, thus a quicker runoff, with early peak than in constant intensity simulated rainfall events having the same duration. The latter effect is also found in this study, where low values of rainfall triangularity (thus a high concentration of the event) coupled with the rainfall burst location and rainfall asymmetry, resulting in a decreased ponding time. Similar conclusions have been found by Frauenfeld and Truman (2004).

Table 5
Coefficients of Eq. (7) fitted considering Δ*uNSI* and saturation or return period. 95% confidence bounds, R^2 and RMSE are also shown. Each coefficient has been classified according to a Natural Breaks Classification. The groups are labelled High (H), Medium-High (MH), Medium-Low (ML) and Low (L).

	$soil_G$	a	a $CI_{95\%}$	a levels	b	b $CI_{95\%}$	b levels	R^2	RMSE		
	$\Delta uNSI = f(Rp)$										
'ALB1'	G1	−2.30	−3.45	−1.15	L	−0.0079	−0.021	0.006	L	0.60	0.74
'VAN1'	G2	−1.16	−1.39	−0.94	MH	0.0006	−0.002	0.003	H	0.09	0.18
'CAP1'	G3	−0.57	−0.69	−0.45	H	0.0033	0.002	0.005	H	0.82	0.10
'FRA1'	G2	−0.57	−0.69	−0.45	MH	0.0033	0.002	0.005	ML	0.82	0.10
'ZIE1'	G3	−0.51	−0.71	−0.31	H	0.0011	−0.003	0.005	MH	0.10	0.16
'LCM1'	G1	−1.69	−1.76	−1.62	L	−0.0002	−0.001	0.000	L	0.17	0.06
'SSI1'	G3	−1.38	−1.43	−1.33	H	−0.0007	−0.001	0.000	H	0.79	0.04
'VED1'	G1	−1.38	−1.43	−1.33	ML	−0.0007	−0.001	0.000	ML	0.79	0.04
'VMO1'	G3	−0.79	−1.25	−0.32	H	0.0032	−0.002	0.008	H	0.36	0.40
'CPE1'	G2	−0.86	−0.89	−0.83	ML	−0.0006	−0.001	0.000	MH	0.76	0.02
	$\Delta uNSI = f(Sat)$										
'ALB1'	G1	−1.70	−2.69	−0.72	L	−0.135	−1.034	0.764	ML	0.05	0.45
'VAN1'	G2	−1.13	−1.86	−0.39	MH	0.115	−0.831	1.060	H	0.02	0.35
'CAP1'	G3	−0.67	−0.90	−0.43	H	0.102	−0.407	0.611	H	0.07	0.11
'FRA1'	G2	−0.70	−1.01	−0.40	ML	0.497	−0.082	1.075	H	0.59	0.16
'ZIE1'	G3	−0.76	−1.21	−0.31	H	−0.665	−1.775	0.445	H	0.36	0.19
'LCM1'	G1	−1.32	−1.71	−0.94	L	0.393	−0.001	0.787	L	0.66	0.19
'SSI1'	G3	−0.73	−1.14	−0.32	MH	−0.704	−1.788	0.380	H	0.40	0.18
'VED1'	G1	−0.86	−1.08	−0.65	L	0.702	0.384	1.021	MH	0.92	0.12
'VMO1'	G3	−1.16	−1.55	−0.76	H	−0.346	−0.914	0.223	MH	0.40	0.18
'CPE1'	G2	−0.57	−0.77	−0.36	ML	0.633	0.171	1.096	ML	0.79	0.11

As well (Dunkerley, 2012) found the longest average time to runoff was related to 'late peak' events followed by 'uniform' events. 'Early peak' events shed runoff more quickly, and 'early peak-gap' event (in which the peak is very close to the start of the event) yielded the shortest time to runoff. This research further observed the effects of storm properties on different soil groups. Overall, the general behaviours described independently from soils are maintained in all simulations. However, differences have been found for the number of peaks in permeable soils (G3). Frequent multi-peak events in average or almost saturated AMC resulted in a delayed runoff production for these soils. This was also highlighted in relation to rainfall regularity: more regular rainfalls with multiple peaks for frequent or rather frequent events increased the ponding time. (Mei and Anagnostou, 2015) found that multi-peak runoff event timing properties are in general taking larger values and wider value ranges than those of the single-peak ones. Frauenfeld and Truman (2004) speculated that many of the differences between different events might be accounted for in terms of greater tendency to soil surface sealing arising in the higher peak intensity of the variable-intensity events. Higher surface permeability might also exist in the uppermost soil of 'uniform' events (Dunkerley, 2012). Thus, soil surface sealing should not be expected for regular events, especially in the more permeable soils, hence the lower ponding time for multi-peak regular rainfalls.

3.3. ΔuNSI *vs return time and saturation*

Eq. (7) was fitted to the values of Δ*uNSI* and return period (Fig. 8a) or saturation (Fig. 8b). Table 5 reports the estimated *a* and *b* coefficients obtained for each soil type, as well as the goodness of fits.

When considering the relationship with the return period (Fig. 7a) testing the value of R^2 for this equation with a two-tailed Student's *t*-test at $\alpha = 0.05$ shows there is a significant relationship between the two variables. Values of *a* range from −2.2 to −0.5 with the lowest value related to ALB1 and the highest one to ZIE1. According to the natural breaks classification, Low values of *a* (a_L) are related only to zones with soils ALB1, a_{ML} is for VAN1, LCM1, SS1 and VED1, a_{MH} is for VMO1 and CPE1, while the higher levels a_H are for CAP1, FRA1, ZIE1. In this case, there is no correlation between the values of *a* and the soil properties, this because the Δ*uNSI* is also influenced by the network properties. The values of *b* range from −0.0079 to 0.0033. The level classification attributes low values of *b* to areas with the ALB1 soil. b_{ML} is for VAN1, LCM1, SS1 and VED1, b_{MH} is for ZIE1, while the higher levels b_H are for CAP1, FRA1, VMO1. Different levels of *b* imply that, for the same *a*, soils having b_L have a watershed response (Δ*uNSI*) about 30 min quicker in 2010 respect 1924, while soils with b_H have a response about 1 h quicker. As well, changes in the magnitude of the events for soils with b_L produce more visible effects, with a reduction of the *uNSI* to about 30 min for the rare VS the frequent events. Soils in b_H instead have a difference of only 20 min. By observing both *a* and *b* at the same time (Fig. 7a), ALB1 appears to be isolated, even if both confidence bounds overlap with the other soils. One must note that ALB1 is the soil where the most significant urbanisation happened over the years, and the network conformation changed the most.

By using the group classification proposed for the ponding time, in the Δ*uNSI* realm soils in G1 are bounded by a_L and $b_{ML\text{-}L}$. Soils in G2 are more scattered and are bounded by $a_{ML\text{-}H}$ and $b_{ML\text{-}H}$, soils in G3 are bounded in b_{MH} and a_{ML}.

According to the proposed model (Eq. (7)), and considering the average *a* and *b* per soil group, G1 has an average Δ*uNSI* of about 1 h, whereas soils in G3 have an average Δ*uNSI* of about 30 min. This indicates that soils in G1, together with being more prone to runoff (see the previous chapter), have witnessed a more significant change in the network response, with a much quicker response in 2010 Vs. 1924. As well, the areas with soils in G1 have a much higher sensitivity to changes in the magnitude of the events, with rare events increasing the changes of up 30 min, respect to less than 10 min for the areas with soils in G2 and G3. Higher changes are expected for frequent events (−1 h), for soils in G1 respect to G3, rather than for rare events (−22 min).

Considering saturation (Fig. 7b) testing the value of R^2 for this equation with a two-tailed Student's *t*-test at $\alpha = 0.05$ shows there is a significant relationship between the two variables, except for the soils ALB1, VAN1 and CAP1. These three are the soils of the areas that have been mostly modified during the years, thus saturation plays a lower role in the watershed response, compared to modification of the network itself, confirming what found in Sofia and Tarolli (2017). When considering the saturation condition, the scaling coefficient (*a*) overlaps with that of Eq. (7) fitted for the Return period, while the exponent (*b*) has a larger order of magnitude. Values of *a* range from −1.7 to −0.5 with the lowest value related to ALB1 and the highest one to CPE1. According to the natural breaks classification, Low values of *a* (a_L) are related only to the soil ALB1, a_{ML} is for VAN1, LCM1, VMO1, a_{MH} is for VED1 and

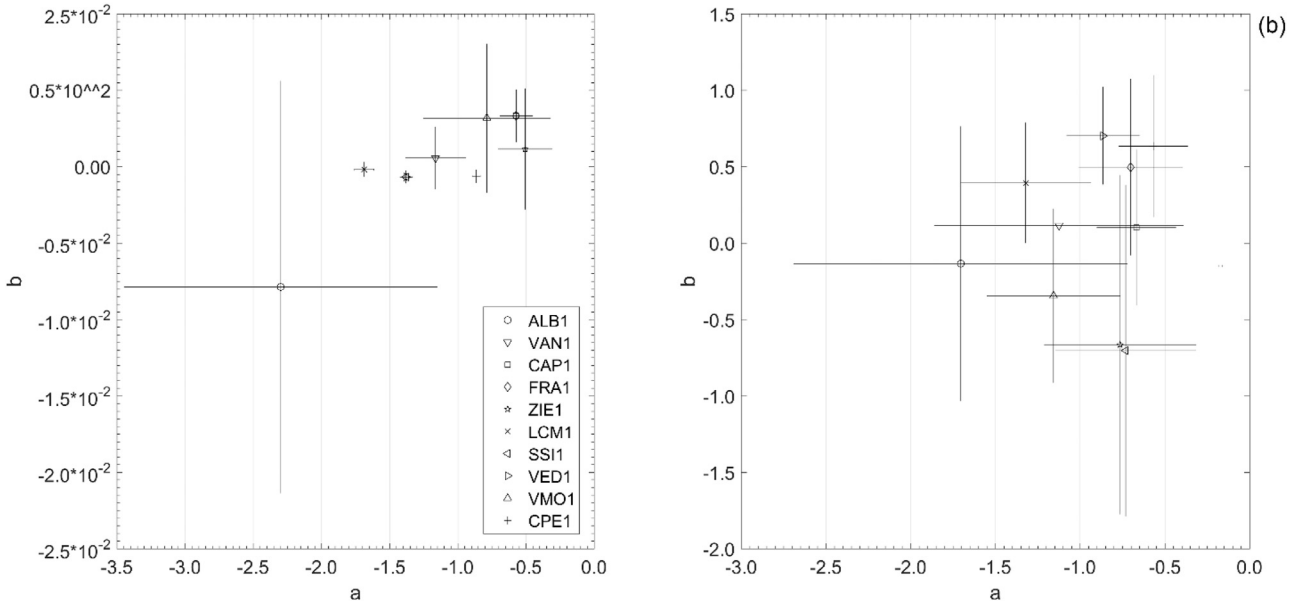

Fig 7. Coefficient of the power law equation for each soil type between Δ*uNSI* and (a) return time and (b) saturation. 95% confidence bounds are also shown.

ZIE1, while the higher levels a_H are for CAP1, FRA1, SSI1, CPE1. Differences in *a* indicate that soils having a_L vs a_H have greater changes in the watershed response, with an average of 1 h and 45 min Vs. 40 min.

Considering *b*, values range between −0.704 to −0.702. The level classification attributes lower *b* (b_L) to ss1 and zie1, b_{ML} to ALB1 and VMO1, b_{MH} VAN1 and CAP1, and b_H to CPE1,VED1,LCM1,FRA1. Soils with b_L have a lower change in the network response respect soils in b_H. However, they have a higher sensitivity to changes in the AMC, with an anticipation of 40% for wet soils Vs. dry soils, Vs a delay of about 60% in the same situation for soils having b_H. The latter effect could be explained by increases in the network properties (higher storage capacity, for example) in 2010 respect 1924 in these areas.

According to the proposed model (Eq. (7)), and considering the average *a* and *b* per soil group, the different soil groups varying sensitivity to changes in saturation, with areas with G1 soils enhancing the network response for saturated Vs. dry soils (Δ*uNSI* is 30 min greater) respect G3 soils (~15 min difference). More significant differences are expected for entirely saturated soils, thus highlighting how network properties play a critical role in runoff production: Δ*uNSI* is 1 h and 15 min greater for G1 vs G3, respect a difference of 30 min in dry conditions.

3.4. ΔuNSI, *network changes, interstorm variability and soil*

According to the AIC approach, the best model describing variations in the Δ*uNSI* respect to the considered drivers is expressed by Eq. (9)

$$\begin{aligned}\Delta uNSI \sim\ & Soil_G + BrLoc_{\%} + Br_n + TRN + asym + \Delta FD + \Delta Stor_{cap} \\ & + \Delta Drain_d + Soil_G : BrLoc_{\%} + Soil_G : Br_n + Soil_G : TRN \\ & + BrLoc_{\%} : TRN + Soil_G : asym + Soil_G : BrLoc_{\%} : TRN \\ & + BrLoc_{\%} : asym + TRN : asym + TRN : asym : \Delta FD \\ & + Soil_G : \Delta FD + Br_n : \Delta FD + TRN : \Delta FD + asym : \Delta FD \\ & + Soil_G : \Delta Stor_{cap} + TRN : \Delta Stor_{cap} \\ & + \Delta FD : \Delta Stor_{cap} + Soil_G : \Delta Drain_d + \Delta FD : \Delta Drain_d \\ & + \Delta Stor_{cap} : \Delta Drain_d + Soil_G : BrLoc_{\%} : asym \\ & + Soil_G : TRN : \Delta FD + TRN : asym : \Delta FD + Soil_G : \Delta FD \\ & : \Delta Stor_{cap} + Soil_G : \Delta FD : \Delta Drain_d + Soil_G : \Delta Stor_{cap} : \Delta Drain_d \\ & + \Delta FD : \Delta Stor_{cap} : \Delta Drain_d + Soil_G : \Delta FD : Stor_{cap} : \Delta Drain_d \end{aligned} \quad (9)$$

The final model has a residual standard error of 0.51 on 2026° of freedom (DF), multiple R^2 of 0.66, Adjusted R^2 of 0.65, F-statistic: 61.27 on 64 and 2026 DF and *p*-value: < 2.2E-16. Compared to the model before the AIC approach, Eq. (8) reduces the residual standard error (−0.01), increases the R^2 (+0.23), increases F (+50), and it increases the degrees of freedom (+247), thus effectively removing excessive to estimate the parameters' variability.

Storm properties as independent drivers are always significant in average (Table 6). *TRN* and Br_n become not significant for high magnitude events in saturated soils conditions. This means that they become not significant when the watershed response is completely controlled by the network properties, rather than by the soil properties. *asym*, on the other hand, is not significant for rare events and saturated soils, or for frequent events in saturated conditions. This means that the rainfall asymmetry has no influence for frequent events when the network controls completely the watershed response, or when frequent events more than likely saturate entirely the soils (the magnitude of the event is large). Indeed *asym* had been shown to have no significant effect on ponding time, as displayed in Table 5.

Storm properties interact with soil, but for frequent events (Rp 2 year), the location of the peak, the number of peaks and the regularity of the rainfall are not significantly correlated with soil groups when the network properties control the response (Sat. 100%) completely. As an independent predictor, the drainage density does not have a significant average correlation with Δ*uNSI*, and it appears to be significant only for frequent events (Rp 2 year), independently from the AMC. On the other hand, difference in storage capacity $\Delta Stor_{cap}$ are significant only when the magnitude of events increases (Rp > = 50 year) for increasing AMC (Sat = 100%). They become highly important for frequent event, instead, when they offer the only storage available (soil is completely saturated) (Table 6). This because low magnitude events on dry soils will saturate the available soil storage, rather than the network one. Difference in the network fractal dimension Δ*FD* are always significant, independently from the saturation or the return time of the event. These behaviours are maintained when network parameters interact with soils (Table 6). Network and storm properties also interact, with relationships between the number of bursts or triangularity and the network fractal dimension.

Increasing soil permeability (G1 to G3) generally delay the watershed response. However, there are instances where increased permeabil-

Table 6
P-values of the statistical significance of the percentage of the total storm period that has occurred at the start of the heaviest burst ($BrLoc_{\%}$), number of bursts (Br_n), hyetograph triangularity (*TRN*), asymmetry of the storm (*asym*), storage capacity $\Delta Stor_{cap}$, drainage density $\Delta Drain_d$, fractal dimension ΔFD, and their interaction (labelled with:) on the average $\Delta uNSI$ (avg), or on the $\Delta uNSI$ of each considered saturation (sat) and return period (RT). For clarity, only values with statistical significance at $p < 0.05$ have been reported.

			Sat. 0%			Sat. 50%			Sat. 90%		
		avg	2	50	200	2	50	200	2	50	200
	soil	2E-248	2E–39	6E-103	2E-05	2E-118	1E–24	6E-09	3E-156	8E-80	1E-77
climate	$BrLoc_{\%}$	8E-13	5E–26	5E-07	9E-29	8E-40	2E–15	7E-38	5E-26	4E-57	3E-21
	Br_n	4E-18	7E–33	2E-03	3E-23	3E-26	4E–14	9E-42	3E-38	5E-12	–
	TRN	3E-12	3E–38	8E-05	6E-13	1E-41	4E–13	2E-40	2E-39	5E-12	–
	asym	3E-05	6E–09	1E-13	–	1E-17	2E–03	5E-03	–	3E-47	3E-27
	$BrLoc_{\%}$:TRN	2E-06	8E–32	6E-33	2E-21	7E-30	2E–25	6E-07	1E-10	4E-65	7E-32
	$BrLoc_{\%}$:asym	2E-07	5E–09	8E-04	1E-02	2E-15	–	2E-03	3E-02	2E-04	1E-02
	TRN:asym	5E-07	1E–08	–	3E-04	9E-03	7E–06	–	1E-04	4E-06	9E-07
network	ΔFD	5E-194	4E–33	4E-62	1E-39	5E-36	1E–59	4E-34	8E-158	2E-106	2E-111
	$\Delta Stor_{cap}$	5E-18	–	1E-02	6E-15	–	3E–09	1E-16	3E-24	2E-12	8E-13
	$\Delta Drain_d$	–	1E–02	–	–	1E-02	–	–	9E-04	–	–
	ΔFD: $\Delta Stor_{cap}$	–	–	–	2E-02	–	–	–	–	–	–
	ΔFD: $\Delta Drain_d$	1E-02	6E–03	2E-02	2E-05	9E-03	6E–07	2E-07	–	–	–
	$\Delta Stor_{cap}$: $\Delta Drain_d$	3E-02	–	–	–	–	3E–02	–	–	–	–
	ΔFD $\Delta Drain_d$: $\Delta Stor_{cap}$	6E-05	–	5E-08	–	–	2E–03	–	9E-04	2E-02	2E-02
climate + network	Br_n: ΔFD	8E-04	2E–04	–	3E-06	–	2E–03	4E-09	6E-03	2E-04	3E-02
	TRN: ΔFD	1E-02	1E–19	2E-02	1E-02	4E-09	1E–02	3E-06	9E-04	–	4E-02
	asym: ΔFD	–	–	–	–	–	–	–	–	–	–
	TRN: $\Delta Stor_{cap}$	–	–	7E-03	–	–	–	–	–	1E-02	–
	TRN:asym: ΔFD	3E-03	–	2E-02	1E-03	2E-02	4E–04	3E-03	–	–	–
climate network and soil	$soil_G$: $BrLoc_{\%}$	1E-15	2E–09	2E-20	2E-33	7E-14	1E–31	1E-32	–	1E-11	4E-09
	$soil_G$: Br_n	4E-19	8E–10	4E-11	4E-12	7E-06	2E–15	1E-10	–	2E-10	5E-06
	$soil_G$:TRN	4E-37	4E–19	2E-28	6E-52	8E-12	1E–53	2E-16	–	7E-08	3E-04
	$soil_G$:asym	4E-03	1E–02	7E-03	1E-05	7E-06	3E–03	3E-16	1E-02	2E-06	9E-08
	$soil_G$: $BrLoc_{\%}$:TRN	1E-09	1E–11	3E-32	5E-45	4E-07	6E–26	3E-45	2E-03	2E-11	7E-09
	$soil_G$: $BrLoc_{\%}$:asym	8E-03	1E–03	1E-03	2E-07	1E-06	7E–06	1E-06	–	–	–
	$soil_G$: ΔFD	1E-22	3E–05	1E-03	1E-15	1E-05	1E–06	1E-23	5E-14	1E-14	2E-13
	$soil_G$: $\Delta Stor_{cap}$	1E-35	–	2E-14	4E-21	–	3E–23	2E-11	3E-44	1E-16	7E-19
	$soil_G$: $\Delta Drain_d$	–	1E–02	–	–	3E-07	–	–	2E-03	–	–
	$soil_G$:TRN: ΔFD	4E-03	3E–03	2E-05	2E-03	2E-04	2E–04	3E-02	–	–	–
	$soil_G$: ΔFD: $\Delta Stor_{cap}$	2E-06	–	–	6E-03	–	–	3E-05	6E-09	2E-06	9E-07
	$soil_G$: ΔFD: $\Delta Drain_d$	1E-14	6E–05	5E-07	2E-08	1E-04	2E–07	4E-04	4E-07	7E-08	6E-06
	$soil_G$: $\Delta Stor_{cap}$: $\Delta Drain_d$	1E-11	–	2E-04	4E-02	3E-02	3E–04	–	5E-03	4E-05	4E-05
	$soil_G$: ΔFD: $\Delta Stor_{cap}$: $\Delta Drain_d$	4E-02	5E–04	–	2E-02	7E-04	1E–03	–	1E-04	2E-02	2E-02

ity (G1 to G3) anticipates the watershed response, namely in the case of multipeak events with regular intensity, or single peak intense events (Fig. 8a), or late peak intense (Fig. 8b) or negatively skewed storms (Fig. 8c).

When considering soil permeability together with network properties (Fig. 8d–f), decrease permeability (G3 to G1) matters mostly for decreasing losses of superficial storage with simultaneous high losses in fractal dimension, or high losses in storage and low losses in fractal dimension (Fig. 8e). In the case of events with regular intensity, however, decrease permeability delays the network response if changes in network patterns (ΔFD) are low (Fig. 8e). Extreme simultaneous changes in storage capacity and network fractal dimension (deltas are high, Fig. 8f) are related to a delay in the response for permeable soils (Fig. 8f). The more permeable soils (G3) produces quicker runoff when changes in the network properties in terms of storage and fractal dimension are low (Fig. 8f). Independently from soil properties, the three network parameters (Fig. 8g), extreme modifications during time (deltas are high) quicken the watershed response. However, if the network patterns are not modified too much ($\Delta Drain_d$ and ΔFD are low), a loss of superficial storage ($\Delta Stor_{cap}$ is high) is critical in reducing the timing to runoff production (Fig. 8g).

This interaction between network parameters changes depending on soil type (Fig. 9).

If all network parameters are drastically altered (deltas are high), soil imperviousness enhances the quickening of the watershed response. However, when the loss of superficial storage is less critical (deltas moving towards low) and so is the loss of complexity of the network patterns (ΔFD), high changes in the drainage density controls the watershed response, making permeable soils the most critical (anticipation of the timing) (right-hand side of the bottom row, in Fig. 9).

The interactions described above changes in relation to soil saturation and event magnitude (Fig. 10).

In average, independently from the other drivers, the delay of the rainfall peak is the parameters that mostly determine a delay in the watershed response. Differently, the highest anticipation in runoff production is due to high changes in fractal dimension related to multipeak events, high changes in storage capacity related to events with regular intensity, and high changes in drainage density together with an increase in soil permeability. For frequent events, as saturation increases, changes in the network parameters are those determining the strongest anticipation in the watershed response. However, when the magnitude of the events is high (Rp 200 year), the strongest control on the watershed response is given by the network mostly in the case of dry soils.

3.4.1. Similarities with previous findings

Independently from the network properties, this research also showed that interstorm variability influence the watershed response. Confirming other findings in the literature (Guan et al., 2016; Qin et al., 2013; Yao et al., 2016), the rainfall peak location has significant effects on runoff. For average return times, events with late peaks in impervious areas have been shown to produce runoff more quickly than in the past. (Yao et al., 2016) findings confirm these results, highlighting how in urban watersheds, lag time decreased the more delayed the rainfall peak was. When using swales for flood reduction, (Qin et al., 2013) observed a reduction of flood attenuation capacity the more delayed the peak was. This is similar to the proposed analysis, where are as having

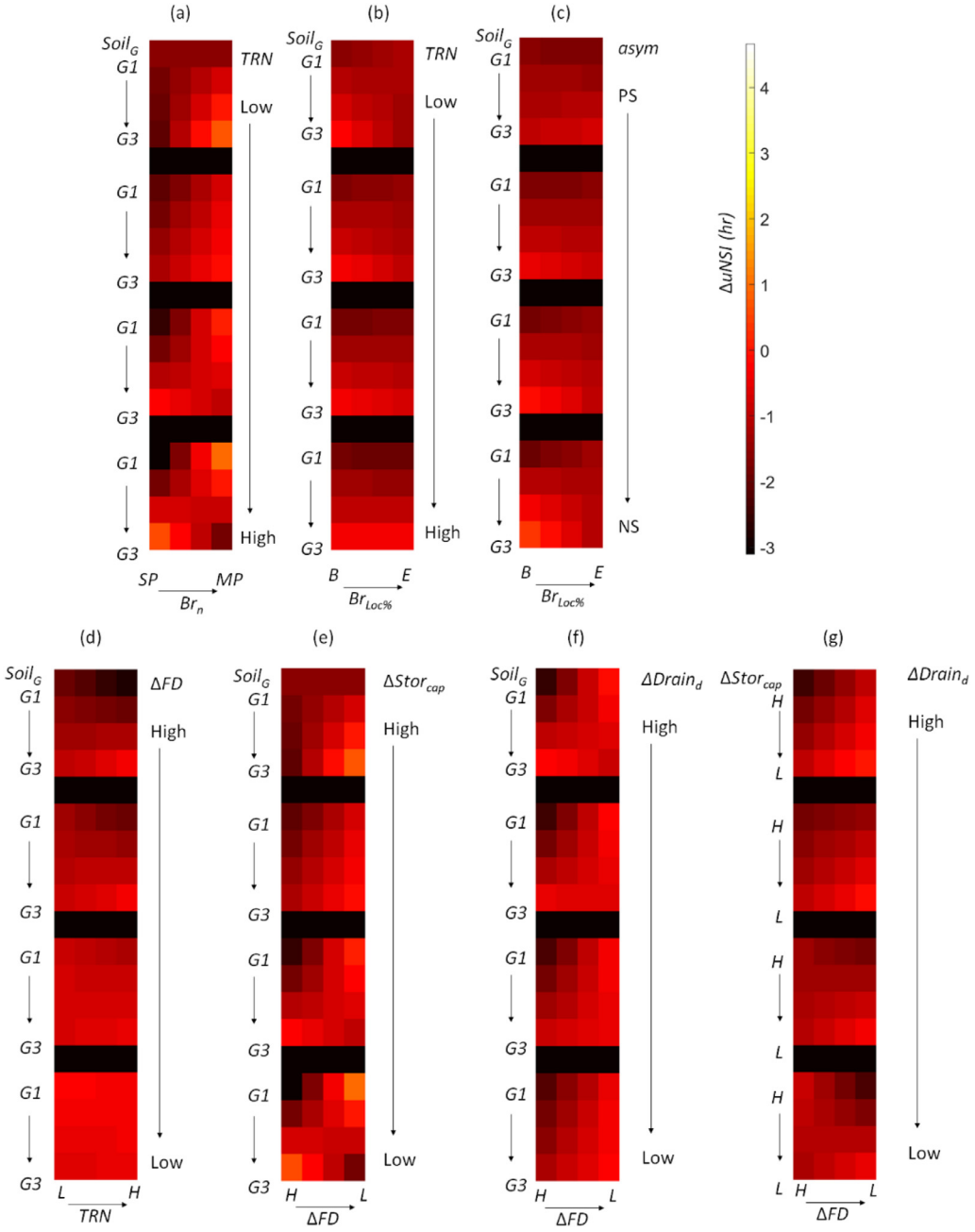

Fig. 8. The plots show the average (for all saturations and return periods) estimated effect on the response of the Δ*uNSI* (in hours) from changing each predictor value: (a) $Soil_G$: Br_n: *asym*; (b) $Soil_G$: $BrLoc_{\%}$: *TRN*; (c) $Soil_G$: $BrLoc_{\%}$: *asym*; (d) $Soil_G$: *TRN*: Δ*FD*; (e) $Soil_G$: Δ*FD*: $\Delta Stor_{cap}$; (f) $Soil_G$: Δ*FD*: $\Delta Drain_d$; (g) $\Delta Stor_{cap}$: Δ*FD*: $\Delta Drain_d$. The considered predictors are asymmetry (*asym*), percentage of the total storm period that has occurred at the start of the heaviest burst ($BrLoc_{\%}$), triangularity (*TRN*) and Soil groups ($Soil_G$) defined as G1 and G3 according to chapter 3.1 (G2 is represented by intermediate pixels between these two). Asymmetry has been defined as Negatively-Skewed (NS), Right-Centred (RC), Left-Centred (LC), and Positively-skewed (PS). $BrLoc_{\%}$has been defined as Beginning (B) and End (E), but intermediate pixels between the two represent FH and SH. *TRN* has been defined as Low (L), and High (H), but intermediate large squares between the two are Medium-Low (ML) and Medium-High (MH).

more permeable soils presented decreased differences in the network response the more the rainfall peak was delayed in time. Considering the network changes and the network response connected to the soil properties, (Sofia and Tarolli, 2017) found that in maximum soil saturation conditions (AMC > 90%), network properties completely control the watershed response, and changes are most evident for the lowest return period. This research highlighted that, as a single predictor, the loss of drainage density matters only during frequent events, while the storage capacity matters when soil offers reduced storage. This is in line with what found in (Miller et al., 2014), where little distinction in hydrological response existed between urban and peri-urban developments of similar impervious cover when no significant hydraulic alteration (network change) was present. As a new parameter, the reduction of the fractal dimension implies a simplification of the network shape and sinuosity. The presented results highlighted that a loss in fractal dimension over time always influences the watershed response, with more similar responses the more similar the network shape is. This is in line with what the literature for floodplain areas highlighted. More sinuous networks reduce peak flows and flooding (Seo et al., 2015; Seo and Schmidt, 2012), and that smaller heterogeneity of path lengths results in higher

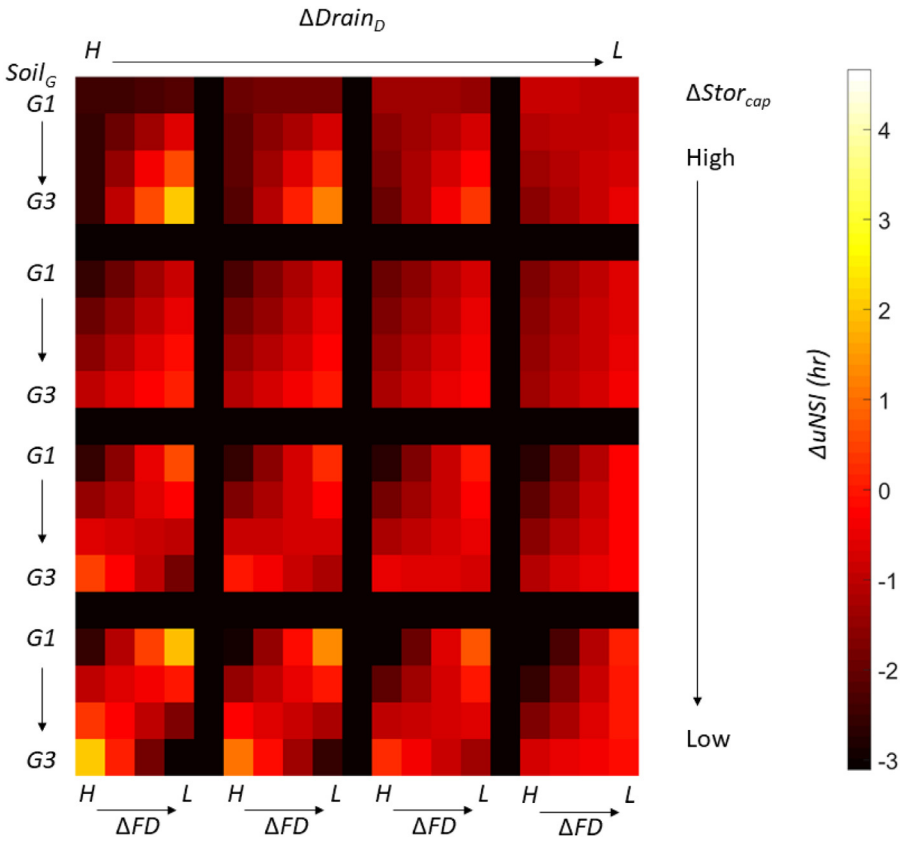

Fig. 9. The plots show the average (for all saturations and return periods) estimated effect on the response of the Δ*uNSI* (in hours) from changing each predictor value: $Soil_G$: Δ*FD:* $Stor_{cap}$: $\Delta Drain_d$. Soil groups ($Soil_G$) are defined as G1 and G3 according to chapter 3.1 (G2 is represented by intermediate pixels between these two), the network parameters changes are labelled as Low (L) and High (H). Medium-Low and Medium-High values are represented by intermediate pixels between the ones represented.

peak flow, a shorter time to peak, and shorter duration (Saco and Kumar, 2002). As well, flood frequency/event increases with the decrease of the fractal dimension of the rivers network (Zhang et al., 2015), indicating that the geomorphologic complexity of rivers network has an important effect on flooding. This research further highlighted the importance of such changes in relation to soil type and storm properties. In average-low AMC, simpler networks (decreased fractal dimension) results in quicker runoff production especially with an increase of the volume of water falling before the heaviest burst and high concentration of the event. The analysis done here showed that rainfall intensification and network shape (Fractal dimension) interact differently depending on soil type.

During frequent events, concentrated rainfalls tend to produce a quicker response in areas with soils prone to saturation and with decreased network complexity. However, when the event magnitude increases, they have the quickest response when rainfall is regular. Zones with higher permeability, instead, always present the quicker response to highly concentrated events, the simpler the network is. Similarly, previous works highlighted how the shape of hydrographs is determined by interlocking relations between the geometry of the network and temporal and spatial variations of precipitation reaching and traversing a graphically specified network (Surkan, 1969). As well, that the relationship between storm speed and direction and the change in the peak runoff is dependent on the network configuration and network efficiency (Seo and Schmidt, 2012). These considerations together with the proposed study highlight the importance of focussing on the network shape parameter in the current climatic context of rainfall intensification (Cortesi et al., 2012; Monjo and Martin-Vide, 2016; Sofia et al., 2017). This research highlighted that all network parameters interact, with different outcomes depending on soil type. Simplified networks, with lowered efficiency (storage capacity) and path heterogeneity (drainage density), presents the quicker response, independently from the soil type. When soils are prone to runoff, and the network efficiency is increased, the watershed response can be delayed in time. When soils have elevated permeability, and the network has a reduced efficiency and path heterogeneity, increasing the network simplicity would result in similar outcomes. As well, if the path heterogeneity and network efficiency are increased, for a given network sinuosity, the watershed response would be delayed. This highlight an important suggestion for flood management: increasing rainfall infiltration and storage capacity (Bens et al., 2007; Marshall et al., 2009), or increasing the ways storms can traverse a specified network, can help mitigate the effects of land use changes.

4. From land drainage to flood management: unravelling the chaos

Currently, there is much policy interest in the possible linkages that might exist between land use, climate and flood risk (Alfieri et al., 2015; Blöschl et al., 2017; European Parliament and Council, 2007; Feyen et al., 2011; Pattison and Lane, 2012; Schneider et al., 2011). On the one hand, this position is sustained by observations from plot- and field-scale studies that suggest land management does affect runoff (Macklin and Lewin, 2015). On the other hand, at larger spatiotemporal scales, two key factors that lead to the intensification of floods during times are the intensification of causative rainfall and changes in the wetness conditions before rainfall (Grillakis et al., 2016; Hlavcova et al., 2005; Woldemeskel and Sharma, 2016), and in many catchments, soil moisture dependent precipitation excess has been found to be much better predictors of the flooding responses than regional patterns and variability of annual flows (Berghuijs et al., 2016). Clearly, establishing a link is difficult because of the need to disentangle hydrological response due to anthropogenic changes of the landscape from that due to natural and possible human-induced rainfall changes. As discussed in the paper, multiple previous findings from different disciplines (hydrology, physical geography) confirmed the findings of this paper in relation to the importance of soil, storm properties, or land use changes in runoff pro-

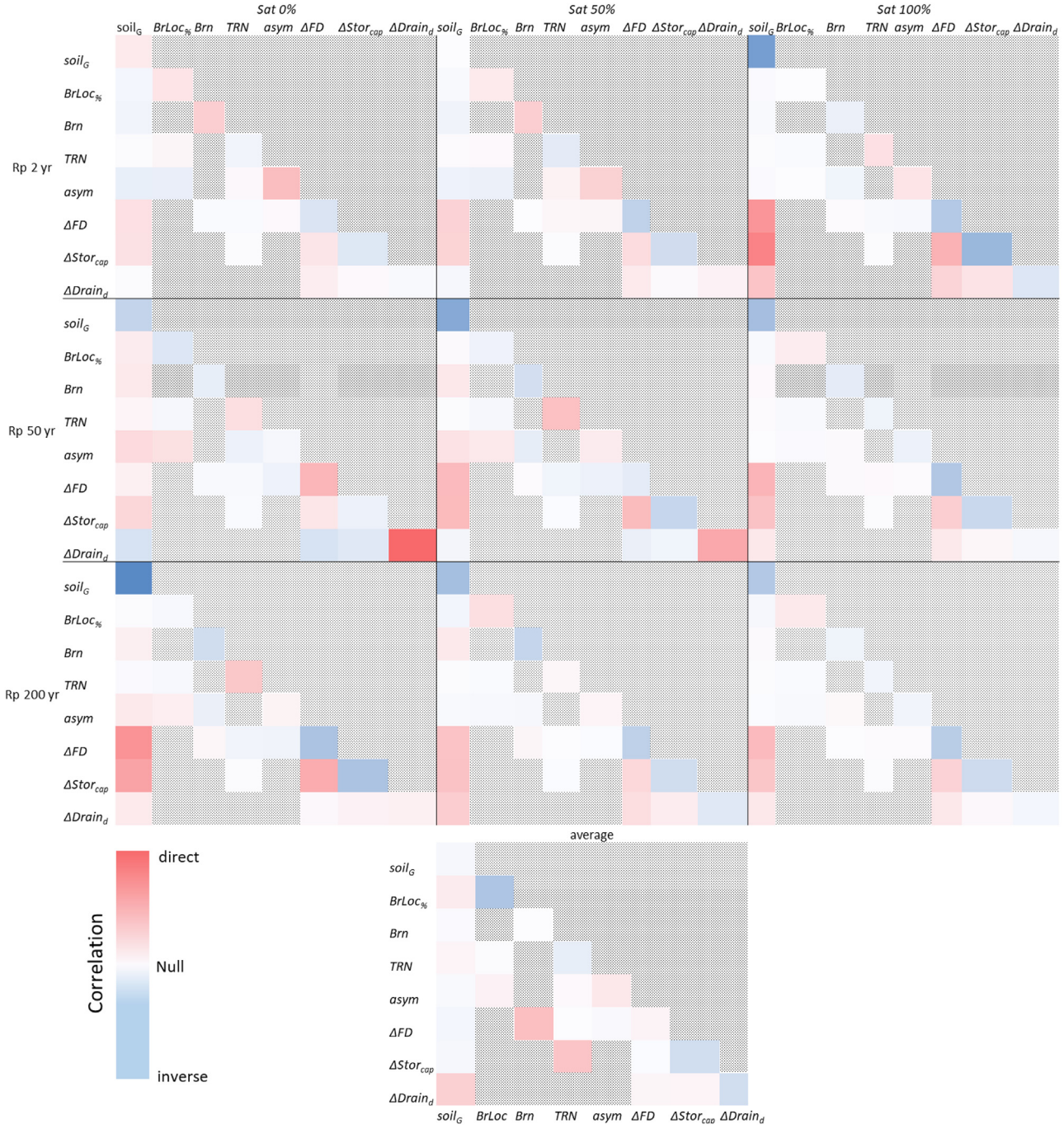

Fig. 10. The plots show the correlation between Δ*uNSI* (in hrs) different saturations (Sat) or return period (Rp) as compared to different classes of storage capacity ($\Delta Stor_{cap}$), drainage density ($\Delta Drain_d$), fractal dimension Δ*FD*, asymmetry (*asym*), percentage of the total storm period that has occurred at the start of the heaviest burst ($BrLoc_{\%}$), number of bursts (Br_n) triangularity (*TRN*), and soil type. Red gradient toward darker colors imply a stronger direct correlation, that is a change in the mentioned parameter(s) determine an anticipation in the watershed response. Similarly, blue gradients towards lighter colors imply a stronger inverse correlation, that is a change in the parameter(s) determine delay of the watershed response. No correlation is represented in white (For interpretation of the references to color in this figure legend, the reader is referred to the web version of this article.).

duction. However, putting together those independent findings and descriptive relationships remained 'chaotic', because such an effort would have cut across actual chains of causations, and would have not captured the sensitive dependence of those linkages upon the specific catchment, scale and event under consideration. This paper, at the scale of the city political boundaries, shows that if there is a relationship between land-use management and watershed response it is through the interaction of a range of processes, some of which are event specific. The assessed results show that not only does a particular change of the drainage in a rural landscape during time has to be carefully investigated with respect to the geography of the catchment (soil type), but whether or not this change has impacts will end up depending upon the temporal evolution of the rainfall event under consideration. This observation shifts the current perspective on historical changes of the landscape, that are generally investigated with an overall aim of identifying a universal answer to the question of the link between a specific land-use measure, storm variability and watershed response.

The results presented in this work have a wide range of implications. Measuring extreme flow events is complex, and most flood observations already contain a mix of measurement and theory (Pattison and Lane, 2012). As a consequence, the relationship between land use and flood characteristics is generally showed as simple correlations between the two factors. The proposed analysis considers realistic soil data and network structures (including the time evolution of such structure), and identifies ponding time and watershed responses on the basis of these actual data as compared to storm characteristics. The application of Eq. (7) to different soil types confirms that runoff production and ponding time, independently from the soil characteristics, follow a common law in nature (power law), but it further demonstrates that soil properties play an important role in this, providing a new insight on the scaling of such relationship to different study areas, or for landscape evolution analysis and flood modeling. The beginning of the effective rainfall in modeling approaches could be now based on such power laws, to simulate events at different magnitude or for different AMC. Further, the development of Eqs. (8) and (9) provides a physical insight on the storm properties controlling the most runoff production, and they disentangle the range of processes, some of which are event specific, that overall control changes in the watershed response. This opens new research lines on the importance of land-use and climate variability influencing flood generating conditions over timescales of societal relevance. Generalising their field of action, despite comprising a large number of variables, exemplifies the fact that land-use effects (network changes) are not mutually exclusive from climate change impacts. Describing the land-use link to flooding has proved difficult, since impact has to be disentangled from the climate-change effect (Pattison and Lane, 2012; Sofia et al., 2017). Many recent studies highlighted how climate is moving toward more intense events with anticipated peaks (Cortesi et al., 2012; Feyen et al., 2011; Monjo and Martin-Vide, 2016; Woldemeskel and Sharma, 2016). This work, analysing storm characteristics such as its triangularity, asymmetry and the peak location, together with soil properties and drainage network changes, highlights how it is likely that land-use changes could amplify the effect of climatic variability. At present it is thought that land-use change effects are of second-order importance behind natural climatic variability (O' Connell et al., 2004, 2007), but this research hints to the fact that land-management policies (through a correct planning and management of new or existing networks) might be also used to mitigate the effect of climate variability on increasing flood risk.

Overall, the proposed analysis show that changes in the same land-management practice (in terms of network structure) will have different effects depending on where it has implemented, and also when implemented in the same location may have different impacts on different flood events due to unique spatio-temporal patterns of precipitation, and soil properties. The effect of this specific land management entity (network structure), furthermore, may also change as different processes and interactions emerge. For example, network changes follows both urbanisation and changes in agricultural mechanisation (Sofia and Tarolli, 2017). Modern techniques include heavy machinery being used, and this can lead to surface roughness collecting runoff (Tarolli et al. 2019), and possibly to a reduction of the hydraulic conductivity of soils (Coutadeur et al., 2002). It is possible for these process impacts to exist at the local scale and interact with the changes in climate, soil characteristics, and network properties, and this should be further investigated.

5. Final remarks

This study analysed the combined product of the storm variability and watershed geomorphology, in controlling water fluxes in an agricultural floodplain area. In this landscape, the configuration of the network layout is not automatically or naturally determined by the topography, but rather by operational choices due to irrigation, urbanisation, or reclamation purposes. The results showed that flooding could arise as a combined product of the storm properties, soil type and network properties. Combining the results from previous studies, this study showed that it is necessary to consider the planning of the layout of the drainage network with intent because it does have a relationship with the watershed response. As well, the network layout cannot be taken into consideration without a correct awareness of the different soil properties. To mitigate the effects of land use changes, in a changing climate where concentrated weather events are expected to generate a larger number of floods, land managers should focus on understanding and improving the surface soil permeability. This could be accomplished either by increasing the rainfall infiltration and storage capacity, or by modifying the ways storms reach and traverse a specified network. Future research work should also keep into account information about groundwater level, and soil crusting and compaction due to different agricultural techniques, to improve the understanding of these potential drivers in increasing flooding risk.

Acknowledgments

LiDAR data were provided by the Ministry for Environment, Land and Sea (Ministero dell'Ambiente e della Tutela del Territorio e del Mare, MATTM), within the framework of the "Extraordinary Plan of Environmental Remote Sensing" (Piano Straordinario di Telerilevamento Ambientale, PST-A). The authors thank the "Servizio Osservatorio Suolo e Bonifiche" of the ARPAV (Agenzia Regionale per la Prevenzione e Protezione Ambientale del Veneto—Environmental Protection Agency of Veneto region) for providing the information about soil characteristics of the study area. The presented study was partially funded by the University of Padova research project DOR1611555 "Water resources management in agricultural landscapes" and CPDR147412 "Drainage networks analysis in anthropogenic landscapes".

References

Abbs, D.J., 1999. A numerical modeling study to investigate the assumptions used in the calculation of probable maximum precipitation. Water Resour. Res. 35, 785–796. https://doi.org/10.1029/1998WR900013.

Akaike, H., 1987. Factor analysis and AIC. Psychometrika 52, 317–332. https://doi.org/10.1007/BF02294359.

Akaike, H., 1981. Likelihood of a model and information criteria. J. Econom. 16, 3–14. https://doi.org/10.1016/0304-4076(81)90071-3.

Alfieri, L., Feyen, L., Dottori, F., Bianchi, A., 2015. Ensemble flood risk assessment in Europe under high end climate scenarios. Glob. Environ. Chang. 35, 199–212. https://doi.org/10.1016/j.gloenvcha.2015.09.004.

ARPAV, 2015. Carta Dei Suoli Del Veneto 1:50.000. ARPAV-Osservatorio Regionale Suolo. Castelfranco Veneto (TV).

ARPAV, 2011. Valutazione Della Permeabilità e Del Gruppo Idrologico Dei Suoli Del Veneto. Osservatorio Regionale Suolo.

Backes, A.R., Bruno, O.M., 2012. Fractal and multi-scale fractal dimension analysis: a comparative study of Bouligand–Minkowski method. Dimens. Contemp. Ger. Arts Lett.

Bens, O., Wahl, N.A., Fischer, H., Hüttl, R.F., 2007. Water infiltration and hydraulic conductivity in sandy cambisols: impacts of forest transformation on soil hydrological properties. Eur. J. For. Res. https://doi.org/10.1007/s10342-006-0133-7.

Berghuijs, W.R., Woods, R.A., Hutton, C.J., Sivapalan, M., 2016. Dominant flood generating mechanisms across the United States. Geophys. Res. Lett. 43, 4382–4390. https://doi.org/10.1002/2016GL068070.

Besussi, E., Cecchini, A., Rinaldi, E., 1998. The diffused city of the Italian North-East: identification of urban dynamics using cellular automata urban models. Comput. Environ. Urban Syst. 22, 497–523. https://doi.org/10.1016/S0198-9715(98)00022-2.

Blöschl, G., Hall, J., Parajka, J., Perdigão, R.A.P., Merz, B., Arheimer, B., Aronica, G.T., Bilibashi, A., Bonacci, O., Borga, M., Čanjevac, I., Castellarin, A., Chirico, G.B., Claps, P., Fiala, K., Frolova, N., Gorbachova, L., Gül, A., Hannaford, J., Harrigan, S., Kireeva, M., Kiss, A., Kjeldsen, T.R., Kohnová, S., Koskela, J.J., Ledvinka, O., Macdonald, N., Mavrova-Guirguinova, M., Mediero, L., Merz, R., Molnar, P., Montanari, A., Murphy, C., Osuch, M., Ovcharuk, V., Radevski, I., Rogger, M., Salinas, J.L., Sauquet, E., Šraj, M., Szolgay, J., Viglione, A., Volpi, E., Wilson, D., Zaimi, K., Živković, N., 2017. Changing climate shifts timing of European floods. Science 357, 588–590. https://doi.org/10.1126/science.aan2506.

Bonell, M., Bruijnzeel, L.A., 2009. Forests, Water, and People in the Humid Tropics : Past, Present and Future Hydrological Research For Integrated Land and Water Management. Cambridge University Press.

Botter, G., Bertuzzo, E., Rinaldo, A., 2010. Transport in the hydrologic response: travel time distributions, soil moisture dynamics, and the old water paradox. Water Resour. Res. 46. https://doi.org/10.1029/2009WR008371.

Bouwer, H., 1966. Rapid field measurement of air entry value and hydraulic conductivity of soil as significant parameters in flow system analysis. Water Resour. Res. https://doi.org/10.1029/WR002i004p00729.

Brakensiek, D.L., Rawls, W.J., Stephenson, G.R., 1984. Modifying SCS hydrologic soil groups and curve numbers for rangeland soils. ASAE Paper. No. PNR-84-203, American Society of Agricultural Engineering, St. Joseph, MI.
Brath, A., Montanari, A., Moretti, G., 2006. Assessing the effect on flood frequency of land use change via hydrological simulation (with uncertainty). J. Hydrol. 324, 141–153. https://doi.org/10.1016/j.jhydrol.2005.10.001.
Casenave, A., Valentin, C., 1992. A runoff capability classification system based on surface features criteria in semi-arid areas of West Africa. J. Hydrol. 130, 231–249. https://doi.org/10.1016/0022-1694(92)90112-9.
Cazorzi, F., Fontana, Dalla, G., De Luca, A., Sofia, G., Tarolli, P., Fontana, G.D., Luca, De, A., Sofia, G., Tarolli, P., 2013. Drainage network detection and assessment of network storage capacity in agrarian landscape. Hydrol. Process. 27, 541–553. https://doi.org/10.1002/hyp.9224.
Cerdà, A., 1998. Relationships between climate and soil hydrological and erosional characteristics along climatic gradients in Mediterranean limestone areas. Geomorphology 25, 123–134. https://doi.org/10.1016/S0169-555X(98)00033-6.
Chin, A., O'Dowd, A.P., Gregory, K.J., 2013. Urbanization and River Channels. Treatise Geomorphol 9, 809–827. https://doi.org/10.1016/B978-0-12-374739-6.00266-9.
Chow, V.Te, Maidment, D.R., Mays, L.W., 1988. Applied Hydrology. McGraw-Hill.
Coelho, R.C., Costa, L.D.F., 1996. On the application of the Bouligand-Minkowski fractal dimension for shape characterisation. Appl. Signal Process.
Cook, R.D., 1979. Influential observations in linear regression. J. Am. Stat. Assoc. https://doi.org/10.1080/01621459.1979.10481634.
Cortesi, N., Gonzalez-Hidalgo, J.C., Brunetti, M., Martin-Vide, J., 2012. Daily precipitation concentration across Europe 1971–2010. Natl. Hazards Earth Syst. Sci. 12, 2799–2810. https://doi.org/10.5194/nhess-12-2799-2012.
Coutadeur, C., Coquet, Y., Roger-Estrade, J., 2002. Variation of hydraulic conductivity in a tilled soil. Eur. J. Soil Sci. 53, 619–628. https://doi.org/10.1046/j.1365-2389.2002.00473.x.
Cronshey, R., 1986. Urban hydrology for small watersheds, 2nd edition. Technical Release No. 55 (TR-55). USDASCS, Washington DC.
David, A., Vassilvitski, S., 2007. K-means++: the advantages of careful seeding. In: Proceedings of the Eighteenth Annual ACM-SLAM Symposium on Discrete Algorithms, pp. 1027–1035.
Dennis, J.E., John, E., Schnabel, R.B.Society for Industrial and Applied Mathematics, 1996. Numerical Methods For Unconstrained Optimization and Nonlinear Equations. Society for Industrial and Applied Mathematics, Philadelphia, PA SIAM, 3600 Market Street, Floor 619104.
Downer, C.W., Ogden, F.L., 2003. Prediction of runoff and soil moistures at the watershed scale: effects of model complexity and parameter assignment. Water Resour. Res. 39. https://doi.org/10.1029/2002WR001439.
Dunkerley, D., 2012. Effects of rainfall intensity fluctuations on infiltration and runoff: rainfall simulation on dryland soils, Fowlers Gap, Australia. Hydrol. Process. 26, 2211–2224. https://doi.org/10.1002/hyp.8317.
Durbin, J., Watson, G.S., 1950. Testing for serial correlation in least squares regression. Biometrika 37, 409–428. https://doi.org/10.1093/biomet/37.3-4.409.
Ellis, E.C., 2011. Anthropogenic transformation of the terrestrial biosphere. Philos. Trans. A. Math. Phys. Eng. Sci. 369, 1010–1035. https://doi.org/10.1098/rsta.2010.0331.
Elsenbeer, H., 2001. Hydrologic flowpaths in tropical rainforest soilscapes–a review. Hydrol. Process https://doi.org/10.1002/hyp.237.
European Parliament and Council, 2007. DIRECTIVE 2007/60/EC on the assessment and management of flood risks. Off. J. Eur. Union.
Fabian, L., 2012. Extreme cities and isotropic territories: scenarios and projects arising from the environmental emergency of the central Veneto città diffusa. Int. J. Disaster Risk Sci. 3, 11–22. https://doi.org/10.1007/s13753-012-0003-5.
Fang, N.-F., Shi, Z.-H., Li, L., Guo, Z.-L., Liu, Q.-J., Ai, L., 2012. The effects of rainfall regimes and land use changes on runoff and soil loss in a small mountainous watershed. CATENA 99, 1–8. https://doi.org/10.1016/j.catena.2012.07.004.
Feyen, L., Dankers, R., Bódis, K., Salamon, P., Barredo, J.I., 2011. Fluvial flood risk in Europe in present and future climates. Clim. Change 112, 47–62. https://doi.org/10.1007/s10584-011-0339-7.
Flerchinger, G.N., Watts, F.J., Bloomsburg, G.L., 1988. Explicit solution to Green-Ampt equation for nonuniform soils. J. Irrig. Drain. Eng. 114, 561–565. https://doi.org/10.1061/(ASCE)0733-9437(1988)114:3(561).
Florida Department of Transportation, 2015. Drainage Manual - IDF Curves and Rainfall Distributions.
Frauenfeld, B., Truman, C., 2004. Variable rainfall intensity effects on runoff and interrill Erosion from two coastal plain Ultisols in Georgia. Soil Sci. 169, 143–154. https://doi.org/10.1097/01.ss.0000117784.98510.46.
Gazzin, A., 2017. 100 Anni Di Cambiamenti Nel Reticolo Idrografico Minore: Importanza Dei Diversi Suoli Nella Risposta Idrologica In Ambiente Agrario. MSc Thesis, University of Padova..
Green, H.W., Ampt, G.A., 1911. Studies on soil phyics. J. Agric. Sci. 4, 1–24. https://doi.org/10.1017/S0021859600001441.
Gregory, K.J., 2006. The human role in changing river channels. Geomorphology 79, 172–191. https://doi.org/10.1016/j.geomorph.2006.06.018.
Grillakis, M.G., Koutroulis, A.G., Komma, J., Tsanis, I.K., Wagner, W., Blöschl, G., 2016. Initial soil moisture effects on flash flood generation – A comparison between basins of contrasting hydro-climatic conditions. J. Hydrol. 541, 206–217. https://doi.org/10.1016/J.JHYDROL.2016.03.007.
Guan, M., Sillanpää, N., Koivusalo, H., 2016. Storm runoff response to rainfall pattern, magnitude and urbanization in a developing urban catchment. Hydrol. Process. 30, 543–557. https://doi.org/10.1002/hyp.10624.
Hlavcova, H., Kohnova, S., Kubes, R., Szolgay, J., Zvolensky, M., 2005. An empirical method for estimating future flood risks for flood warnings. Hydrol. Earth Syst. Sci. 9, 431–448. https://doi.org/10.5194/hess-9-431-2005.
Hodgkins, G.A., Whitfield, P.H., Burn, D.H., Hannaford, J., Renard, B., Stahl, K., Fleig, A.K., Madsen, H., Mediero, L., Korhonen, J., Murphy, C., Wilson, D., 2017. Climate-driven variability in the occurrence of major floods across North America and Europe. J. Hydrol. 552, 704–717. https://doi.org/10.1016/J.JHYDROL.2017.07.027.
Hooke, J.M., 2006. Human impacts on fluvial systems in the Mediterranean region. Geomorphology 79, 311–335.
Huff, F.A., 1967. Time distribution of rainfall in heavy storms. Water Resour. Res. 3, 1007–1019. https://doi.org/10.1029/WR003i004p01007.
Ibbitt, R.P., 1997. Evaluation of optimal channel network and river basin heterogeneity concepts using measured flow and channel properties. J. Hydrol. 196, 119–138. https://doi.org/10.1016/S0022-1694(96)03293-3.
Kalantari, Z., Nickman, A., Lyon, S.W., Olofsson, B., Folkeson, L., 2014. A method for mapping flood hazard along roads. J. Environ. Manage. 133, 69–77. https://doi.org/10.1016/J.JENVMAN.2013.11.032.
Krause, S., Jacobs, J., Bronstert, A., 2007. Modelling the impacts of land-use and drainage density on the water balance of a lowland–floodplain landscape in northeast Germany. Ecol. Modell. 200, 475–492. https://doi.org/10.1016/j.ecolmodel.2006.08.015.
Lado, M., Paz, A., Ben-Hur, M., 2004. Organic matter and aggregate-size interactions in saturated hydraulic conductivity. Soil Sci. Soc. Am. J. 68, 234. https://doi.org/10.2136/sssaj2004.2340.
Macklin, M.G., Lewin, J., 2015. The rivers of civilization. Quat. Sci. Rev. 114, 228–244. https://doi.org/10.1016/j.quascirev.2015.02.004.
Malik, R.S., Butter, B.S., Anlauf, R., Richter, J., 1987. Water penetration into soils with different textures and initial moisture contents. Soil Sci. 144.
Marshall, M.R., Francis, O.J., Frogbrook, Z.L., Jackson, B.M., McIntyre, N., Reynolds, B., Solloway, I., Wheater, H.S., Chell, J., 2009. The impact of upland land management on flooding: results from an improved pasture Hillslope. Hydrol. Process https://doi.org/10.1002/hyp.7157.
Mei, Y., Anagnostou, E.N., 2015. A hydrograph separation method based on information from rainfall and runoff records. J. Hydrol. 523, 636–649. https://doi.org/10.1016/J.JHYDROL.2015.01.083.
Miller, J.D., Kim, H., Kjeldsen, T.R., Packman, J., Grebby, S., Dearden, R., 2014. Assessing the impact of urbanization on storm runoff in a peri-urban catchment using historical change in impervious cover. J. Hydrol. 515, 59–70. https://doi.org/10.1016/J.JHYDROL.2014.04.011.
Monjo, R., Martin-Vide, J., 2016. Daily precipitation concentration around the world according to several indices. Int. J. Climatol. 36, 3828–3838. https://doi.org/10.1002/joc.4596.
Niehoff, D., Fritsch, U., Bronstert, A., 2002. Land-use impacts on storm-runoff generation: scenarios of land-use change and simulation of hydrological response in a meso-scale catchment in SW-Germany. J. Hydrol. 267, 80–93. https://doi.org/10.1016/S0022-1694(02)00142-7.
O'Connell, P.E., Beven, K.G., Carney J.N., Clements, R., Ewen, J., Fowler, H., Harris, G.L., Hollis, J., Morris, J., O'Donnell, G.M., Packman, J.C., Parkin, A., Quinn, P.F., Rose, S.C., Shepherd, M., Tellier, S., 2004. Review of impacts of rural land use and management on flood generation, Report A: Impact Study Report. R&D Technical Report FD2114/TR.
O'Connell, P.E., Ewen, J., O'Donnell, G., Quinn, P., O'Connell, P.E., Ewen, J., O'Donnell, G., Quinn, P., O'Connell, P.E., Ewen, J., O'Donnell, G., Quinn, P., 2007. Is there a link between agricultural land-use management and flooding? Hydrol. Earth Syst. Sci. 11, 96–107. https://doi.org/10.5194/hess-11-96-2007.
Pan, W., 2001. Akaike's information criterion in generalized estimating equations. Biometrics 57, 120–125. https://doi.org/10.1111/j.0006-341X.2001.00120.x.
Pattison, I., Lane, S.N., 2012. The link between land-use management and fluvial flood risk: a chaotic conception? Prog. Phys. Geogr. https://doi.org/10.1177/0309133311425398.
Potter, T.L., Truman, C.C., Strickland, T.C., Bosch, D.D., Webster, T.M., Franklin, D.H., Bednarz, C.W., 2006. Combined effects of constant versus variable intensity simulated rainfall and reduced tillage management on cotton preemergence herbicide runoff. J. Environ. Qual. 35, 1894. https://doi.org/10.2134/jeq2005.0444.
Qin, H., Li, Z., Fu, G., 2013. The effects of low impact development on urban flooding under different rainfall characteristics. J. Environ. Manage. 129, 577–585. https://doi.org/10.1016/j.jenvman.2013.08.026.
Rawls, W.J., Pachepsky, Y.A., Ritchie, J.C., Sobecki, T.M., Bloodworth, H., 2003. Effect of soil organic carbon on soil water retention. Geoderma 116, 61–76. https://doi.org/10.1016/S0016-7061(03)00094-6.
Rinaldo, A., Beven, K.J., Bertuzzo, E., Nicotina, L., Davies, J., Fiori, A., Russo, D., Botter, G., 2011. Catchment travel time distributions and water flow in soils. Water Resour. Res. 47. https://doi.org/10.1029/2011WR010478.
Risse, L.M., Nearing, M.A., Zhang, X.C., 1995. Variability in Green-Ampt effective hydraulic conductivity under fallow conditions. J. Hydrol. 169, 1–24. https://doi.org/10.1016/0022-1694(94)02676-3.
Roder, G., Sofia, G., Wu, Z., Tarolli, P., Roder, G., Sofia, G., Wu, Z., Tarolli, P., 2017. Assessment of social vulnerability to floods in the floodplain of Northern Italy. Weather. Clim. Soc. https://doi.org/10.1175/WCAS-D-16-0090.1.
Ruiz-Constán, A., Ruiz-Armenteros, A.M., Galindo-Zaldívar, J., Lamas-Fernández, F., Sousa, J.J., Sanz de Galdeano, C., Pedrera, A., Martos-Rosillo, S., Caro Cuenca, M., Delgado, J.M., Hanssen, R.F., Gil, A.J., 2017. Factors determining subsidence in urbanized floodplains: evidence from MT-InSAR in Seville (southern Spain). Earth Surf. Process. Landf. 42, 2484–2497. https://doi.org/10.1002/esp.4180.
Saco, P.M., Kumar, P., 2002. Kinematic dispersion in stream networks 1. Coupling hydraulic and network geometry. Water Resour. Res. 38. https://doi.org/10.1029/2001WR000695, 26-1-26–14.
Scherpinski, C., Uribe-Opazo, M.A., Boas, M.A.V, Sampaio, S.C., Johann, J.A., 2010. Spatial variability of hydraulic conductivity and water infiltration in the soil. Acta Sci. https://doi.org/10.4025/actasciagron.v32i1.959.

Schilling, K.E., Helmers, M., 2008. Effects of subsurface drainage tiles on streamflow in Iowa agricultural watersheds: exploratory hydrograph analysis. Hydrol. Process. 22, 4497–4506. https://doi.org/10.1002/hyp.7052.
Schneider, C., Flörke, M., Geerling, G., Duel, H., Grygoruk, M., Okruszko, T., 2011. The future of European floodplain wetlands under a changing climate. J. Water Clim. Chang. 2, 106–122. https://doi.org/10.2166/wcc.2011.020.
Seo, Y., Hwang, J., Noh, S., 2015. Analysis of Urban drainage networks using Gibbs' model: a case study in Seoul, South Korea. Water 7, 4129–4143. https://doi.org/10.3390/w7084129.
Seo, Y., Schmidt, A.R., 2012. The effect of rainstorm movement on urban drainage network runoff hydrographs. Hydrol. Process. 26, 3830–3841. https://doi.org/10.1002/hyp.8412.
Sofia, G., Prosdocimi, M., Fontana, Dalla, G., Tarolli, 2014. Modification of artificial drainage networks during the past half-century: Evidence and effects in a reclamation area in the Veneto floodplain (Italy). Anthropocene 6, 48–62. https://doi.org/10.1016/j.ancene.2014.06.005.
Sofia, G., Roder, G., Fontana, Dalla, G., Tarolli, 2017. Flood dynamics in urbanised landscapes: 100 years of climate and humans' interaction. Sci. Rep. 7. https://doi.org/10.1038/srep40527.
Sofia, G., Tarolli, P., 2017. Hydrological response to ~30 years of agricultural surface water management. Land 6, 3. https://doi.org/10.3390/land6010003.
St. Johns river water management district, 2010. Management and storage of surface waters.
Surkan, A.J., 1969. Synthetic hydrographs: effects of network Geometry. Water Resour. Res. 5, 112–128. https://doi.org/10.1029/WR005i001p00112.
Svensson, C., Jones, D.A., 2010. Review of rainfall frequency estimation methods. J. Flood Risk Manag. 3, 296–313. https://doi.org/10.1111/j.1753-318X.2010.01079.x.
Tarolli, P., Sofia, G., 2016. Human topographic signatures and derived geomorphic processes across landscapes. Geomorphology 255, 140–161. https://doi.org/10.1016/j.geomorph.2015.12.007.
Tarolli, P., Sofia, G., CAO, W., 2018. The Geomorphology of the Human Age, in: Encyclopedia of the Anthropocene. Elsevier, pp. 35–43. https://doi.org/10.1016/B978-0-12-809665-9.10501-4.
Tarolli, P., Cavalli, M., Masin, R., 2019. High-resolution morphologic characterization of conservation agriculture. CATENA 172, 846–856. https://doi.org/10.1016/j.catena.2018.08.026.
Ungaro, F., Calzolari, C., Busoni, E., 2005. Development of pedotransfer functions using a group method of data handling for the soil of the Pianura Padano–Veneta region of North Italy: water retention properties. Geoderma 124, 293–317. https://doi.org/10.1016/j.geoderma.2004.05.007.
Ungaro, F., Calzolari, C., Pistocchi, A., Malucelli, F., 2014. Modelling the impact of increasing soil sealing on runoff coefficients at regional scale: a hydropedological approach. J. Hydrol. Hydromech. 62, 33–42. https://doi.org/10.2478/JOHH-2014-0005.
Upton, G.J.G., Cook, I., Ian, T.Oxford University Press, 2008. A Dictionary of Statistics. Oxford University Press.
van den Elsen, E., Hessel, R., Liu, B., Trouwborst, K.O., Stolte, J., Ritsema, C.J., Blijenberg, H., 2003. Discharge and sediment measurements at the outlet of a watershed on the Loess plateau of China. CATENA 54, 147–160. https://doi.org/10.1016/S0341-8162(03)00062-6.
Viero, D.P., Peruzzo, P., Carniello, L., Defina, A., 2014. Integrated mathematical modeling of hydrological and hydrodynamic response to rainfall events in rural lowland catchments. Water Resour. Res. 50, 5941–5957. https://doi.org/10.1002/2013WR014293.
Wasko, C., 2014. Quantile regression for investigating scaling of extreme precipitation with temperature. Wat. Resour. Res. 50. https://doi.org/10.1002/2013WR015194.
Wasko, C., Sharma, A., 2015. Steeper temporal distribution of rain intensity at higher temperatures within Australian storms. Nat. Geosci 8, 527–529.
Wheater, H., Evans, E., 2009. Land use, water management and future flood risk. Land policy 26, S251–S264. https://doi.org/10.1016/j.landusepol.2009.08.019.
Wilson, B.N., Sheshukov, A., Pulley, R., 2006. Erosion Risk Assessment Tool For Construction Sites-Final Report.
Woldemeskel, F., Sharma, A., 2016. Should flood regimes change in a warming climate? the role of antecedent moisture conditions. Geophys. Res. Lett. 43, 7556–7563. https://doi.org/10.1002/2016GL069448.
Xiao, L., Hu, Y., Greenwood, P., Kuhn, N., 2015. A combined raindrop aggregate destruction test-settling tube (RADT-ST) Approach to identify the settling velocity of sediment. Hydrology 2, 176–192. https://doi.org/10.3390/hydrology2040176.
Yao, L., Wei, W., Chen, L., 2016. How does imperviousness impact the urban rainfall-runoff process under various storm cases? Ecol. Ind. 60, 893–905. https://doi.org/10.1016/J.ECOLIND.2015.08.041.
Yevjevich, V., 1992. Water and civilization. Water Int. 17, 163–171. https://doi.org/10.1080/02508069208686135.
Zhang, Q., Xu, C., Gemmer, M., Chen, Y.D., Liu, C., 2009. Changing properties of precipitation concentration in the Pearl River basin, China. Stoch. Environ. Res. Risk Assess. 23, 377–385. https://doi.org/10.1007/s00477-008-0225-7.
Zhang, S., Guo, Y., Wang, Z., 2015. Correlation between flood frequency and geomorphologic complexity of rivers network - A case study of Hangzhou China. J. Hydrol. 527, 113–118. https://doi.org/10.1016/j.jhydrol.2015.04.060.
Zhang, X.C., Norton, L.D., Hickman, M., 1997. Rain pattern and soil moisture content effects on atrazine and metolachlor losses in runoff. J. Environ. Qual. 26, 1539. https://doi.org/10.2134/jeq1997.00472425002600060013x.
Zhang, Y., Hernandez, M., Anson, E., Nearing, M.A., Wei, H., Stone, J.J., Heilman, P., 2012. Modeling climate change effects on runoff and soil erosion in southeastern Arizona rangelands and implications for mitigation with conservation practices. J. Soil Water Conserv. https://doi.org/10.2489/jswc.67.5.390.